New Approach in Fabrication of Solid-State Nanopore for Bio-Sensing Applications

by

Wing Hei Harold Kwok

Thesis submitted to
The Faculty of Graduate and Postdoctoral Studies
In partial fulfilment of the requirements for the Degree of
Doctorate in Philosophy degree in Physics

uOttawa

"It is only with the heart that one can see rightly;
what is important is invisible to the eye"

The little prince, Antoine de Saint-Exupery

Abstract

The 21st century marks the defining point of human history in terms of technological advancement. In 2014, we were at the edge of acquiring a complete understanding of the fundamental construct to all life forms. The capability to manipulate and recreate lives as desired will soon be at our hands and will eventually lead to the redefinition of life and humanity. This brave new world, for better or worse, will be stitched together by scientific breakthroughs in many disciplines.

Nanopore fluidic system – and microfluidic in general – might be one of the key puzzles towards the future. It is seen as a likely candidate for the next generation of rapid and low-cost genetic sequencing technology, which will allow us to gain thorough insight into the genetic code of every living organism on earth. It can also have the capability to individually detect and manipulate virtually any biological molecules, possibly allowing it to be a universal diagnostic tool or a bio-molecule synthesiser. The future of nanopore fluidic system is prosperous, but the difficulties are equally challenging. Currently, both biological and solid-state nanopores are non-trivial to create. For instance, a small solid-state nanopore can only be fabricated with expansive machinery in a low-yield, low-throughput manner.

To overcome this challenge, a new set of methods involving high electric field to fabricate and enlarge a solid-state nanopore has been developed. It was found that a nanopore, when subjected to a high electric field, can be enlarged in angstrom increments and cleared of unidentified obstructions that cause low-frequency ionic current fluctuations. It was also found that an intact solid-state membrane, when subjected to a high electric field for a period of time, can leave a single nanopore imprinted onto it. The process of creation is best describe as a dielectric breakdown event and can be modeled by the percolation theory for dielectric breakdown. The resulting nanopores are cylindrical in shape and are shown to be equally capable of single molecule sensing compare to pores created by other methods. To accommodate future nanopore designs and applications and to examine the scope of applicability of the new fabrication approach, more advanced nanopore devices were created on some dual-layer solid-state

membranes comprising of a metallic and a dielectric layer. Experiments indicated that the method could indeed create nanopore on such advanced membranes. It was further shown that the metallic layer receded further than the dielectric layer, forming a hollow conical shape at the opening of the dielectric nanopore. Such metalized bi-layer nanopore system was found to interact strongly with short single stranded DNA molecules, resulting in prolonged DNA translocation time. A simple picture of the mechanism was proposed to explain the observation. Lastly, to extend the limit of the new fabrication approach, I attempted to fabricate nanopore on complex multi-layer membranes involving a graphene film sandwiched in several dielectric materials. It was found that the quality of the graphene film and the transfer method were vital to the success of this project. Nevertheless, preliminary results indicated that the new method could create a nanopore through this complex multi-layer membrane.

The new method to fabricate and tune both simple and complex nanopores is amongst the simplest, the least costly and the most efficient one that one can imagine. The research work has already sparked a dramatic increase in scientific throughput in our laboratory and other laboratories we had collaboration with. It fueled more than a dozen projects and involved close to a thousand nanopores in total. Such projects are far from possible if they were to rely on conventional fabrication methods. However, these are insignificant if we consider the new method is simple enough that, for the very first time, general public can easily access nanofabrication and single-molecule manipulation technology. The liberation of nanotechnology to the general public symbolically marks the beginning of a brave new world.

List of Publications

Patents

[P1] **W. H. Kwok**, V. Tabard-Cossa, and K. A. Z. Briggs, "Fabrication of nanopores using high electric fields," WO 2013167955 A12013.

[P2] **W. H. Kwok**, M. Godin, E. Beamish, and V. Tabard-Cossa, "Method for controlling the size of solid-state nanopores," WO 2013167952 A12013.

Journal Articles

[A1] **H. Kwok**, K. Briggs, and V. Tabard-Cossa, "Nanopore fabrication by controlled dielectric breakdown.," *PLoS One*, vol. 9, no. 3, p. e92880, Jan. 2014.

[A2] **H. Kwok**, M. Waugh, J. Bustamante, K. Briggs, and V. Tabard-Cossa, "Long Passage Times of Short ssDNA Molecules through Metallized Nanopores Fabricated by Controlled Breakdown," *Adv. Funct. Mater.*, vol. 24, no. 48, pp. 7745–7753, Oct. 2014.

[A3] E. Beamish, **H. Kwok**, V. Tabard-Cossa, and M. Godin, "Precise control of the size and noise of solid-state nanopores using high electric fields.," *Nanotechnology*, vol. 23, no. 40, p. 405301, Oct. 2012.

[A4] E. Beamish, **H. Kwok**, V. Tabard-Cossa, and M. Godin, "Fine-tuning the size and minimizing the noise of solid-state nanopores.," *J. Vis. Exp.*, no. 80, p. e51081, Jan. 2013.

[A5] K. Briggs, **H. Kwok**, and V. Tabard-Cossa, "Automated Fabrication of 2-nm Solid-State Nanopores for Nucleic Acid Analysis.," *Small*, vol. 10, no. 10, pp. 2077–86, May 2014.

[A6] Briggs, K.; Charron, M.; **Kwok, H.**; Le, T.; Chahal, S.; Bustamante, J.; Waugh, M.; and Tabard-Cossa, V., "Kinetics of Nanopore Fabrication by Controlled Breakdown of a Dielectric Membrane in Solution," accepted to Nanotechnology

[A7] Waugh, M.; Carlsen, A.; Sean, D.; Slater, G.; Briggs, K.; **Kwok, H.**; and Tabard-Cossa, V., "Interfacing Solid-State Nanopores with Gel Media to Slow DNA Translocations." Submitted to Electrophoresis

Media Coverage

[*]Anderson, A. (2014, March 18). Team Describes Method for Fabricating Solid-State Nanopores With Modified Electrical System. *Genomeweb*. Retrieved from https://www.genomeweb.com/sequencing/team-describes-method-fabricating-solid-state-nanopores-modified-electrical-syst

This Week in PLOS. (2014, March 24). *Genomeweb*. Retrieved from https://www.genomeweb.com/blog/week-plos-281

Zhao, Q. (2014, June 18). Sub 2-nm solid-state nanopores: smaller pores can see more. *Materials Views*. Retrieved from http://www.materialsviews.com/sub-2-nm-solid-state-nanopores-smaller-pores-can-see-more/

Software

[SW1] **Kwok, H**. NanoFabricator. (2014). at <https://sourceforge.net/projects/nanofabricator/>

[SW2] **Kwok, H**. NanoID. (2014). at <https://sourceforge.net/projects/nanoid/>

[SW3] **Kwok, H**. Resistive-Pulse Analyzer. (2014). at <https://sourceforge.net/projects/resistivepulseanalyzer/>

Conference

[C1] **H. Kwok**, K. Briggs, and V. Tabard-Cossa, "Rapid fabrication of sub-5nm solid-state nanopore for low cost biosensing," *APS March Meet. 2013*, vol. 58, no. 1, p. N44.00010, 2013. [Oral Presentation]

[*] The report did not correctly describe the origin of the discovery. It was not serendipitous as the article tried to portray. To the best of my knowledge, no one has investigated the scenario of discovery by any mean.

Statement of Originality and Contribution

I hereby declare that this thesis results from my own independent investigation and that, to the best of my knowledge, chapters 4-6 constitute original researches of important scientific value. There are additional works not part of this thesis, which are directly resulted from my contribution. Originality of this thesis and other contributions are discussed in detail in the following sections.

Originality and Remarks

Research in the course of my study began with a self-initiated project on improving the protocol of handling a TEM drilled nanopores for electrophoretic experiments. This was motivated by the high failure rate in the use of TEM drilled nanopore. Failure refers to high fluctuation in ionic current when a nanopore is submerged in electrolyte. A multitude of attempts have been tested, including aggressive chemical cleaning, extensive electrolyte purification and applying a high voltage bias. Conceptually it is known that high voltage can damage a nanopore in a fluidic environment, but what I discover was that the damage can be small, and that the high ionic fluctuation can be eliminated as a pore is being enlarged. Sharing the discovery with colleagues resulted in publications A3 and A4.

At the time, I was designated to fabricate nanopores with TEM to facilitate research projects in two laboratories. Improving the fabrication method became a personal priority. Immediately after the discovery of the nanopore tuning method, even before mentioning to any other about the discovery, I conceived that it was possible to fabricate a nanopore with a similar approach. Initially, I was seeking a sharp conductive scanning probe as a mean to localize the electric field and the damage. Later, after some literature research, I realized that localization by

physical mean was not necessary. This idea originated from the fact that damages by over-voltage in microelectronic integrated circuits systems were often highly localized, and the damages were in the range of nanometers.

These conceptual constructs led to the first working protocol. The first design relies on connecting a 10V voltage source to a resistor and a pristine membrane in series. The resistor acts as a passive cut-off for the system. When a nanopore is created in liquid and ionic current begins to increase, voltage drop across the resistor would also increase, thus terminating the creation-enlargement process. Soon after the realization of the method, I redesigned the protocol, moving to an active real-time feed-back system presented in chapter 4.

At the time, the fabrication process would take days to create a pore, rendering the method impractical. To solve the problem, I explored different control parameters and found that the creation time of a nanopore strongly depended on the bias voltage and the pH. This discovery allows a nanopore to be fabricated within minutes for the first time, proving the usefulness of the method. Soon after, I demonstrated that such nanopores were capable of performing electrophoretic experiment of DNA molecules. Around the same time, I also identified the fabrication mechanism as a dielectric breakdown process, and explained the phenomenon by the percolation theory. This provided a fundamental understanding of the process, which lead to the development of a control strategy. These works constitutes the major body of chapter 4 and publication A1.

At this point, the project took off and Kyle Briggs joined the project. He provided valuable experimental data in support of the method and had contributed to the research progress. Various other projects rely on this fabrication method were also launched at around the same time, resulted in several other publications. I later initiated other research projects on the basis of the new fabrication method, in respond to the latest advanced research in the field. These projects were predominately constituted by me and are described in Chapter 5 and Chapter 6.

List of Contribution

Individuals involved in the research projects included:

Kyle Briggs, Matthew Waugh, José Bustamante, Eric Beamish,
Prof. Michel Godin, Prof. Vincent Tabard-Cossa

I would like to thank everyone listed here. Your contributions have led to the formulation of this thesis.

Following presents the detail of my contribution to this thesis. I hereby declare, to the best of my ability, that this list isan accurate record.

Chapter 4 & Publication A1

"Nanopore Fabrication by Controlled Dielectric Breakdown"

- Conceived and designed the experiment solely
- Discovered that acidity dramatically influence the fabrication time
- Discovered that high voltage significantly decrease the fabrication time
- Identified the fabrication mechanism as a dielectric breakdown event
- Introduced percolation theory of dielectric breakdown to explain the mechanism
- Demonstrated that such nanopores were capable of detection of DNA molecules
- Demonstrated that the method was compatible with different dielectric materials
- Designed and developed the software, electric circuits and handling protocol for the experiment
- Invented the method to test the wetting status of a membrane with capacitance
- Fabricated nanopores with different salt electrolytes, which helped eliminate other possible creation mechanism involving specific ionic reactions
- Developed a new method to locate a nanopore on a large free standing membrane, under a TEM, which led to the imagining of our nanopores for the first time. It helped to confirm the creation of a single pore and to gain insight into the shape of the pore.
- Conceptualized, collected and visualized the data presented in Figures 4.1-4.7, except Figure 4.4
- Wrote Chapter 4

Chapter 5 & Publication A2

"Long Passage Times of Short ssDNA Molecules through Metallized Nanopores Fabricated by Dielectric Breakdown"

- Conceived and designed the experiment solely
- Conceived and demonstrated that the method could remove both metallized and dielectric layers
- Imaged metallized nanopore under TEM
- Illustrated that the gold formed a conical shape, based on the TEM investigation
- Argued that the metal was removed by electrochemical etching
- Illustrated that such nanopores were capable of electrophoretic detection of DNA molecules
- Illustrated that DNA translocation in such pore were slowed significantly
- Proposed a picture involving the interaction between DNA and metals to explain the experimental data
- Contributed to the design of the holder for gold evaporation
- Conceived, collected and visualized data on Figures 5.1-5.7 and Figures S5.1-S5.3
- Wrote Chapter 5 and Publication A2

Chapter 6

"Fabrication of multilayer graphene-embedded nanopore device"

- Conceived and designed the experiment solely
- Developed the software for three electrode electrophoretic experiments
- Developed the protocol for graphene sandwich membranes
- Conceived, collected and visualized data on Figures 6.1-6.7
- Wrote Chapter 6

Publication A3 & A4

"Precise control of the size and noise of solid-state nanopores using high electric fields"

"Fine-tuning the size and minimizing the noise of solid-state nanopores"

- Discovered the method to enlarge a nanopore
- Discovered the method to remove low frequency ionic fluctuation
- Proposed to use a real-time monitoring current feedback system as the control
- Fabricated nanopores for the experiment with TEM

Chapter 1-3

- Wrote Chapters 1-3
- Section 3.4 was resulted from independent investigation, but might have been documented in the academia.

Other Publications

- Discussed and exchanged ideas to facilitate these projects
- Shared the latest finding on the new fabrication method (before its publication) to facilitate these projects

Acknowledgment

I would like to sincerely thank everyone who has walked with me since the beginning. At times of unspeakable sorrow, and of immense pain, and of arduous struggle with my health condition, your faith in me is my strength to persist. Your pure and truthful love delighted me at times of despair and enmity. Without you, I might not be the person I am now. Special thanks to my dearest wife, thanks for everything. Your care and support during this time are most important to me. I love you very much. To my parents, who makes all these and much more possible. Thank you for inspiring me to be curious about this world, and to think critically, and to resist conformation. It is most regrettable that I cannot finish this study earlier. I miss you a lot. All credit should be designated to you. Lastly, thank you Lord my savior, you are the reason for me to endeavor and to preserve my integrity and dignity, such that I can complete the study without shame or guilt or being in jail.

I would also like to thank my supervisor, Dr. Vincent T-Cossa, for giving me the opportunity to research at your lab. The collaboration was not always smooth, and there were things we could not come to agreement, but the resulting works are something we can always feel proud of. It is a small impact we made to the world – together. Neither can achieve this independently. I would also like to thank Dr. James Harden, who taught most of my graduate courses. Your passion in teaching and theoretical physics is inspiring. You made some changes to how I see equations.

Sincerely, thank you very much!

Table of Contents

List of Figures

List of Acronyms

ALD	Atomic Layer Deposition
CETD	critical electron trap density
DFT	Discrete Fourier Transformation
DI	Di-Ionized (water)
DNA	Deoxyribonucleic acid
dsDNA	double-stranded Deoxyribonucleic acid
EDL	Electrical double layer
EOF	Electroosmotic Flow
FIB	Focused Ion Beam
FIR	Finite Impulse Response
FN	Fowler–Nordheim (Tunneling)
GNR	Graphene Nanoribbon
HIM	Helium Ion Microscope
IIR	Infinite Impulse Response
SEM	Scanning Electron Microscope
SHE	substrate hot electron (Tunneling)
SILC	Stress Induced Leakage Current
ssDNA	single-stranded Deoxyribonucleic acid
TAT	Trap Assisted Tunneling
TDDB	time dependent dielectric breakdown
TEM	Transmission Electron Microscope

Chapter 1

Review and Prospects of Solid-State Nanopore Fabrication Technology

Review and Prospects of Solid-State Nanopore Fabrication Technology

1.1 History and Origin of Nanopore Technology

Nanopores are defined as any physical channels with submicron characteristic dimensions. They usually have a low or medium aspect ratio. When the aspect ratio is high, they share overlapping reference with nanotubes. The most common use of the term refers to small nanopores from a single nanometer to dozens of nanometers in size. These small nanopores are important because they allow the pass-through and sensing of individual molecular analytes. Nanopore-based technology has its origin (in terms of technological advancements) as a small pore hundreds of micron in size. Microfluidic sensing technique utilizing these small pores has been around for half a century. It was first developed for micro-particles analysis in the late 1940's[1,2]. The principle is based on observing an increase in resistance as a particle passes through a pore filled with electrolyte, thus the technique is known as resistive-pulse sensing, and the phenomenon is called the Coulter principle, name after the inventor Wallace H. Coulter. The invention, using micron-sized pore to count particles, was proven to be extremely useful at the time, resulting in the founding of Coulter Corporation. The micro-particle sensing device, known as a Coulter Counter, is still in heavy use today in medical laboratories for cell sorting and counting applications.

After the discovery, the next major advancement in resistive-pulse sensing technology was about 20 years later, following the discovery of track etching technique to fabricate pores. The method involves exposing a polymer membrane to energetic particles from radioactivity. The electronic structures of the membrane material along the trace of particles' trajectory are modified, allowing them to be selectively etched away, leaving some pores on the membrane. The density of pores and

their sizes can be controlled by the exposure dosage and etching conditions. This technique allows a reliable fabrication of single sub-micron pore for the first time. With these sub-micron track-etched pores, DeBlois and Bean extended the precision of Coulter Counter to angstrom scale, allowing them to analyze the size of a submerged virus particle, about 100nm in size, directly[3,4]. The breakthrough provoked great excitement in the field and contributed invaluable understanding to the foundation of virology[3].

At around the same time, the rise of electrophysiology gave a twist to the development of resistive-pulse sensing techniques. Ion-channels are gated nanopores found in nature, few nanometer in size, that reside on lipid membrane of all cells. These channels are responsible for gating molecule transport, which are essential to the functioning of a living cell. To investigate these ion-channels, a unique set of instruments and methodologies was invented, giving rise to the field of electrophysiology. A typical setup involves contacting a cell with a glass micro-pipette tip. Lipids cell membrane forms a good electrical seal with glass rim of the pipette tip, allowing the monitoring of ions exchange across the rim-encircled region of the membrane[5]. Activities of these ion-channels are registered as a small change in current, equivalent in nature to resistive-pulse sensing. Special amplification instruments were built to monitor the minute change in current. The development of electrophysiological method to study a living cell opened a wide door for fundamental researches in cellular biology, which eventually led to a surge of new discoveries and the award of multiple independent Nobel Prizes for Physiology or Medicine in the related researches[6–8]. More importantly, experiments in electrophysiology are virtually identical to resistive-pulse sensing experiments using an organic nanopore. For this reason, studies in nanopore

benefited tremendously from the maturity of electrophysiology. Currently, most groups doing research on nanopore still relies on protocol and amplification electronics developed for electrophysiology.

Since the discovery of nanopore, numerous proposals were suggested as potential applications. Of those suggestions, the idea of utilizing a nanopore to sequence genomic material had caught the most attention. It inspired a multitude of different approaches for the challenge. In general, these approaches can be categorized into two main branches, those that are based on organic nanopores and those that are based on solid-state nanopores. After almost a decade of research, organic nanopores were the first to demonstrate the capability of sequencing DNA[9–11]. A major contributing factor to the triumph of organic over solid-state nanopore was the fact that it can be formed with single atom precision. Through interlocking of a unique sequence of amino acid, each organic nanopore of the same kind is virtually identical and has a well defined geometry. For example, the center of a α-hemolysin nanopore consists in a constricted site 1.4 nm in diameter and about 1 nm in length, where the entire nanopore structure is made of an exact atomic arrangement[12]. In addition, geometry of an organic nanopore can be customized through site directed mutagenesis[13]. For instant, a mutant form of α-hemolysin having two constricted site was reported to improve DNA base recognition[14]. Through mutation process, the geometry, local charge profile, hydrophobilicity, and surface chemistry of an organic nanopore can be customized. Such precision and control is overwhelmingly unmatched even with the latest state-of-the-art nanofabrication technology. This is at the heart of the challenge of current solid-state nanopore research. It illustrated the impending needs of a breakthrough in solid-state nanopore fabrication technology.

1.2 Nanopore fabrication method

1.2.1 Energetic Particle Beam

Energetic beam of particles like electrons and ions were utilized to drill individual nanopore directly. Both electron and ion beams require sophisticated machinery. In the case of electrons, drilling is performed under a transmission electron microscope (TEM), while ion beam drilling is performed with a focused ion beam (FIB) setup, which is usually mounted on a scanning electron microscope (SEM). A newer class of FIB utilizing helium ions provides superior milling resolution to conventional FIB technique that uses heavier gallium ions. In a typical setup, helium FIB drilling is performed with a helium ion microscope (HIM). Both TEM and FIB drilling are similar in principle: they rely on a set of apertures and electromagnetic lens to focus a tight beam of charged particles onto the sample. To achieve a minimum spot size, a beam converges into a spot at an angle. As a result, the beam drills a double cone shape on the membrane[15], as shown in figure 1.1. The double cone geometry introduced an effective thickness, which is less than the thickness of the membrane. This can be desirable or undesirable depending on situations. For instance, by lowering the effective thickness, resistance of a pore is reduced, which translates to better sensitivity and higher signal-to-noise ratio. On the other hand, positioning a focused spot along the thickness on a membrane posted tough control requirement. As a result, yields and reproducibility is very low. In addition, it introduces experimental unknown on the pore geometry, particularly the position of the double cone along the thickness of the membrane, which limits the practicality of these pores. As of the current status, a TEM can reach 2nm in pore diameter, while FIB with Helium ion can reach around 5nm. Other FIB methods can only reach pore diameter around 10nm.

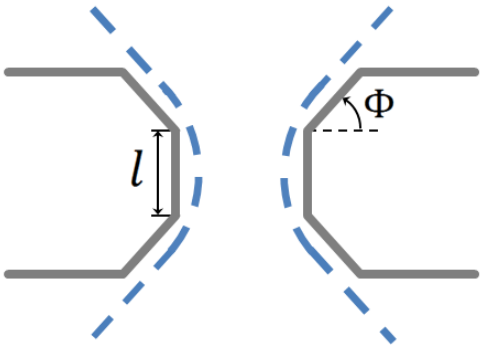

Figure 1.1: Illustration of the geometry of a TEM drilled nanopore. Φ is the angle of convergence of a beam. The Blue dash lines depict the trace of a converging electron beam. Double cone geometry of the beam trace is imprinted onto the nanopore. This introduces an effective length, l, onto the pore, which is less than the thickness of the membrane.

1.2.2 Nanopore Tuning

1.2.2.1 Tuning by Material Reflow

Directly drilling a small nanopore less than 2-nm in diameter is very difficult with TEM, and is unreachable in a reliable manner with other energetic beam drilling method. An alternative approach is to shrink a large pore in a controlled fashion. It can be done by reflow of membrane material or by deposition of additional material. Reflow of material to shrink a nanopore is usually accompanied with energetic beam drilling methods. It was first demonstrated with an Argon ion beam sputtering setup, and the method was termed *ion beam sculpting*[16,17]. The schematic of the apparatus is shown in figure 1.2. As illustrated in the figure, a silicon nitride membrane is fixed on a temperature-controlled holder. Argon ions from an ion gun bombard on the membrane surface. To create a nanopore, a cavity is first introduced to the back side of the membrane via reactive ion etching. Ion bombardment will slowly sputter off material on the front surface; the receding front surface will eventually meet the cavity, forming a large pore. Then, by adjusting the sputtering

condition, the same ion beam is utilized to initiate atomic transport within the membrane, which lets a large pore shrink in a controlled manner, ultimately reaching a few nanometers in size. It is found that the transition between sputtering and shrinking depends on several important parameters, which include[16]: 1) membrane temperature, 2) beam exposure condition (duty cycle of the exposure), and 3) the ion flux of the beam. Shortly follows the report, similar methods based on the same concept are reproduced on FIB[18] and TEM[19] systems. In general, this class of methods requires extensive calibration to gain consistent control. In addition, ions can be implanted onto the membrane, changing the atomic composition and material characteristics[17]. Furthermore, the technique usually requires a thick membrane and is incompatible to ultra thin material like graphene and silicene. It is also incompatible with more complex membranes like multi-layered membranes.

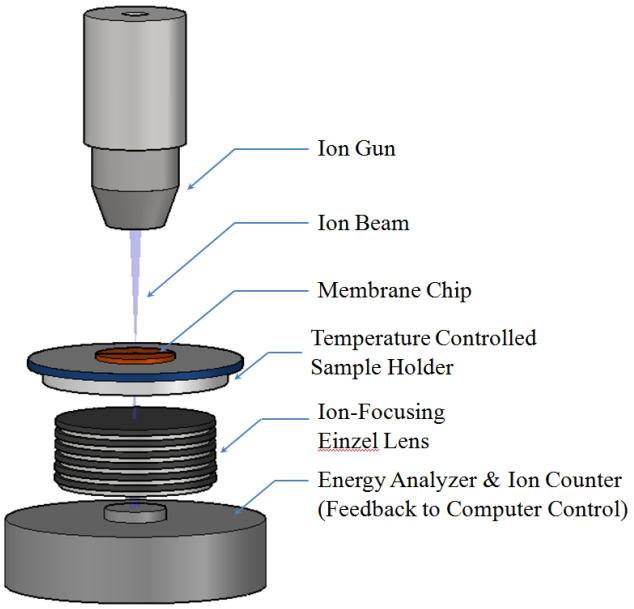

Figure 1.2: Schematic of an ion beam sculpting setup.

1.2.2.2 Tuning by Material Deposition

Beside reflow of membrane material, a nanopore can also be shrunk by depositing additional material in a controlled manner. Atomic layer deposition (ALD) is a material deposition technique that takes advantage of self-limiting chemical-vapor reactions at a surface to deposit inorganic material[20]. Peng *et al.*[21] had shown that such technique can be utilized to shrink a nanopore in a controlled manner. The method relies on depositing material with ALD onto an initially large pore, usually drilled with FIB. The ALD process involves exposing a nanopore membrane with alternating species of chemical vapor reagents. The precursor reagent molecules, containing the atoms to be deposited, rely on surface absorption to be attached onto a sample. Absorption diminishes as the surface is saturated with precursor molecules. This self-limiting mechanism gives rise to the unique property of individual layer deposition in the method. While the surface is saturated with the precursor molecules, a second gas reagent, usually water vapor, is delivered to the sample. The second reagent molecule breaks loose the precursor molecule, leaving the intended atoms deposited onto the surface. Repetition of this process results in atoms being deposited in a layer-by-layer manner. An advantage of using ALD is the fact that the process is highly conformal, which deposit material onto a pore wall at about the same rate as the rest of the surface, until the shrunk pore is comparable to the size of the precursor molecule. Upon which the self-limiting mechanism pitches in, terminating the shrinkage. The self-termination property is crucial to nanopore tuning. It allows unmanaged automata in the tuning process, in strong contrast to all previously discussed methods. Shortly after the first report utilizing ALD to shrink a nanopore, groups have shown that the process is transferrable to wafer-scale process of shrinking an array of nanopores[22]. The method allows a controlled fabrication of 2 nm nanopores in a highly scalable manner for the very first time. However, the method is not without drawbacks. The method still

depends on the precise fabrication of an initial large pore. Furthermore, while a pore is being shrunk, the membrane is being thickened as a trade-off. This translates to a lengthened nanopore, which scarifies sensitivity and restricts signal-to-noise ratios, somewhat defeating the initiative. A more detail discussion on this matter is presented in section 2.3.

1.3 Complex and Integrated Nanopores System

1.3.1 Trend toward Complex System

Despite a decade of research efforts, sequencing of genomic material with resistive-pulse method has not been demonstrated using simple solid-state nanopore device. Several physical limitations have significantly hindered such progress. One major hurdle, mentioned in a previous section, is that the precision of the fabrication is far inferior to the atomic precision required. Similarly, the resolution of a simple nanopore is dictated by the length of a pore. A few nanometers in length correspond to the resistive-pulse sensing of a dozens of nucleotides simultaneously, rendering distinction and identification of a single nucleotide impossible. To address these limitations, groups have attempted to fabricate nanopore on monolayer or multi-layer graphene membranes. However, these devices are still bounded by the increased noise and bandwidth limitation in resistive-pulse experiments[23,24]. These limitations of simple nanopore device motivated research groups to investigate a multitude of different complex nanopore devices as an alternative solution. Some of these complex nanopore devices not only attempted to overcome previously mentioned physical limitations of ionic current sensing, but exploited alternative physical sensing mechanisms to bypass these problems altogether . The abundance of designs renders discussing all of them beyond the scope of this thesis. Several are discussed below to illustrate the current state of active researches in the field.

1.3.2 Integrated microfluidic-electronic system

As mentioned in the previous section, noise is one of the major limitations in resistive pulse sensing. It is partly due to parasitic capacitance from the membrane and electronic elements[25–29] at the pre-amplification input. To reduce such noise, groups built low noise pre-amplification circuit integrated to the nanofluidic device. Rosenstein *et al.* designed a multi-channel CMOS pre-amplication circuit integrated with a voltage-clamped transimpedence circuit and a Ag/AgCl electrode[30]. The conductive path between the electrode and a pre amplification circuit is 100 μm, which is significantly shorter than a typical setup in the order of centimeters. Further fabrication effort was made to minimize the membrane capacitance by using a thick membrane with a locally thinned region where a nanopore would sit on. Amplification circuit was specially designed for high bandwidth low noise purposes. The authors reported a significant reduction in high bandwidth region above 10kHz, compare to a widely used electrophysiology patch clamp amplifier like Axopatch 200B by Molecular Devices. The improved noise performance of the integrated system allows resistive-pulse sensing with a nanopore at the sub-microsecond temporal resolution, at which it is comparable to the translocation speed of individual nucleotides in a DNA molecule. This work demonstrated the advantage of building a complex integrated nanofluidic-electronic device and pointed to a potential route for advancement in nanopore sensing technology.

1.3.3 Organic solid state hybrid nanopore device

Organic molecules have a very high specificity on interaction with other bio-molecules. For instance, an appropriate choice of immunoglobulin (antibody) can be made to bind with a unqiue analyte specifically. This is the basic principle of immunoassay, which is a widely applied technology in the area of medical diagnostic. The precision of molecular structure, complex

functionality, and specificity of molecular binding mechanism are unmatched in solid-state system. For this reason, groups take advantage of these organic molecules by building some organic-solid-state hybrid nanopore devices. Their work demonstrated interesting results and extended the capability of solid-state nanopore system. For instance, Yusko *et al.* reported that coating an aqueous suspension of small unilamellar liposomes on the surface of silicon nitride nanopore can prevent it from clogging[31]. In addition, the existence of a fluidic lipid coating allows further chemical functionalization with lipid-anchored ligands or receptors. The authors showed that these lipid-anchored binding molecules can capture analytes onto the liquid lipid surface and slowly diffuse along the surface into a pore at the present of a voltage bias. The capturing effectively concentrates analytes and therefore dramatically improves sensitivity. Furthermore, motions of these bounded analytes are limited by the viscosity of the lipid bilayer, allowing the detection as they translocate through the pore, which are otherwise too fast to observe. Such capability is very important in medical diagnostic and molecular biology applications.

1.3.4 Advanced Material Integrated System

Advances in material science have facilitated nanopore researches. Groups are using novel materials, like graphene nanoribbons and nanotubes to build complex integrated nanopore devices. These devices take advantage of the special electrical and physical properties of the advanced materials to extend the capability of a nanopore. In doing so, groups are exploring sensing mechanisms beyond the regime of resistive-pulse sensing.

In 2013, Traversi *et al* reported their work on a new integrated nanopore sensor device. The team built a nanopore sensor by integrating a graphene nanoribbon (GNR) with a solid state nanopore[32].

The device consists of a GNR spanning across the opening of a nanopore. It allows the detection of individual DNA plasmid molecules simultaneously with both resistive-pulse sensing current and field effect modulated graphene current. A schematic of the device is shown in figure 1.3. Two metallic electrodes were created to make electrical contact with the GNR. Current driven across the GNR by the two electrodes was monitored. Due to the ambipolar nature of graphene, the GNR can act as either p-type or n-type conductor depending on the gate voltage bias, resulting in either an increase or decrease in graphene current as a charged molecule translocates through the GNR. Currently, the resolution of sensing with GNR is limited by the bandwidth of the system and did not improve in sensitivity over resistive-pulse sensing. However, with the addition of an independent sensing mechanism, it opens up new research opportunities in improving the sensing resolution. The understanding of graphene field-effect current and its noise in a nanofluidic system is still premature and may require years of fundamental researches to improve on the design.

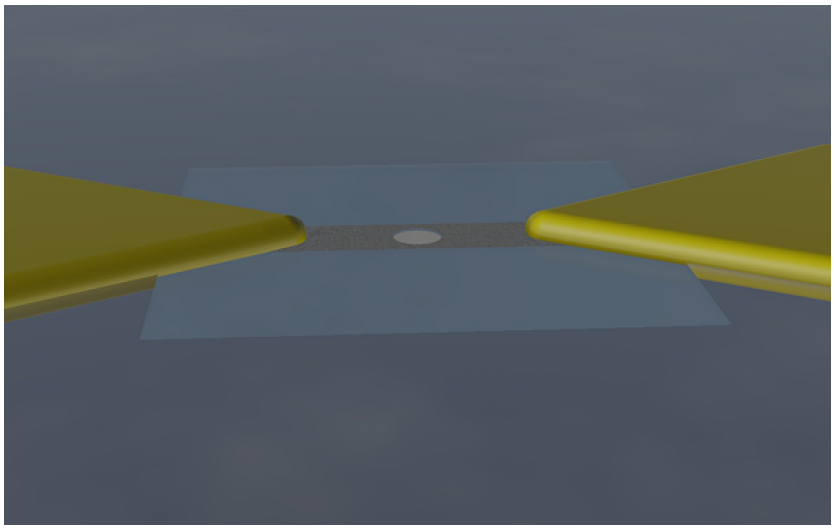

Figure 1.3: Schematic of a graphene nanoribbon nanopore device. A graphene nanoribbon is placed on a free-standing membrane between two metal electrodes. A nanopore is drilled through the ribbon and the free standing membrane. Metal electrodes attached to both ends of the nanoribbon allow charge carry current to pass through the graphene, forming a field effect sensor.

In another report in 2013, researchers Liu *et al*.[33] showed that a short carbon nanotube can be used to replace an organic nanopore, α-haemolysin, for DNA sensing applications. In the experiment, a short single-walled carbon nanotube (SWCNT), about 0.8nm to 2nm in diameter and 5nm to 10nm in length, was placed on a lipid bilayer membrane similar to a typical setup of an organic nanopore system. Liu and co-authors found that ions mobility inside SWCNT increased significantly compare to the bulk. They were able to utilize such system to identify 5-hydroxymethylcytosin (5hmC) in ssDNA molecules, thus extending the application of nanopore to the field of epigenetic researches. The integration of advanced material into a nanopore sensing platform appears to be a current research trend in the field. In the future, these advanced materials might bring new capabilities to current nanopore sensing platform with minimal adaptations.

1.4 Prospect of Future Nanopore Fabrication Technique

Nanofabrication technology has been advancing rapidly during the past decades. In the perspective of history, numerous novel discoveries at the time ended up serving an intermediate purpose only. They were replaced and made obsolete by the rivalry of advancing frontier. Majority of the current nanopore fabrication methods were developed specifically for the creation of small nanopores. They provided precisions of fabrication in the range from angstroms to nanometers, made possible the creation of small nanopore for single molecule sensing, and have facilitated indispensible researches on the understanding in the field. However, specificity of these methods made them incompatible with main stream wafer-scale nanofabrication processes, and is therefore inadaptable to complex integrated devices or large scale production.

Currently, semi-conductor industry relies solely on lithography-based nanofabrication technologies. Such technologies have the advantage of compatibility to all processes essential to nanofabrication, including the deposition, modification and removal of materials in a precise and massively parallel manner. With the proper resist material and etching process, lithography-based technique is capable of producing nanoporous structures[22,34,35]. However, at the moment, both the feature sizes and precision are still about an order away from the requirement for fine sensing of single molecules. For instance, in order to distinguish different bases in a single strand DNA (ssDNA) using resistive-pulse sensing mechanism, it would require the diameter of a pore be close to the diameter of a ssDNA molecule, ~1.4nm, and a precision comparable to the differences in size between different nucleotides, which are in the order of angstroms.

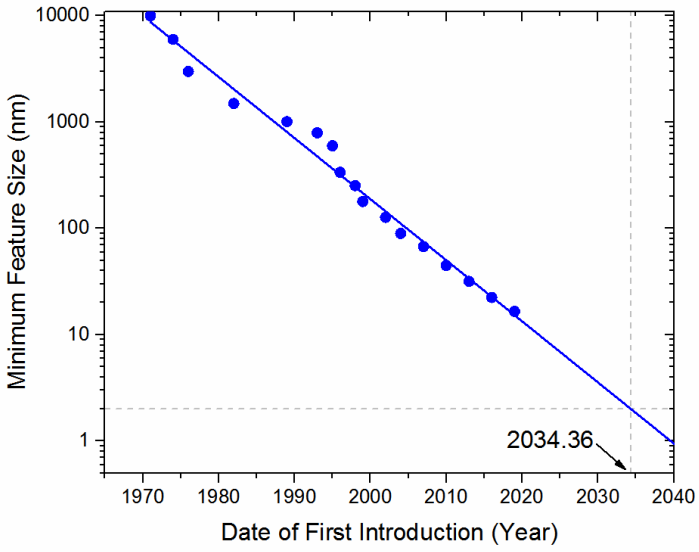

Figure 1.4: Semi-log chart of the minimum feature size of commercialized semiconductor device[36]. The data is fitted with Moore's law (half-time is 5.24yr), and extrapolated into the future. According to this projection, 2nm features will be available commercially by year 2034.

The advancement of lithography-based technology is mainly driven by the huge demand in the consumer market. The mixture of demand, profit and competition fueled a wide discipline of researches aiming dedicatedly to push the limit. As a result, the maturation of the technology follows a well predicted trajectory, nicely modeled by the widely cited Moore's Law[37]. Figure 1.4 illustrates the smallest feature size trend of commercialized product from the industry for the past 45 years[36]. It shows that the smallest feature size has been closely following the power law proposed by Moore during the entire period since the beginning of microfabrication. Projecting into the future, it would take about 20 more years before commercialized litho-based technology reach sub-nanometer precision and produce features 2nm in size. And years before industry adopting a technology, there will be scattered reports from laboratories reporting reaching this resolution with different litho-based approaches. To highlight the current status, here lists some recent reported achievements in the field. In 2003, Gates *et al*. reported replication of 2nm vertical features and 1 Å precision by soft lithography[38]. The following year, Austin *et al.* reported the creation of 5nm line features with 14nm pitch using nanoimprint lithography[39]. In 2014, Pavel *et al*. reported fabricating 1-nm line features using quantum optical lithography[40,41]. The method relies on a special glass ceramic photoresist to achieve sub-wavelength resolution using conventional photolithography setups. These techniques are to be refined and matured before wide-scale adaptation. When this day comes, I firmly believe that litho-based technology would make obsolete current nanopore fabrication methods involving milling with energetic particles or the method relying on dielectric breakdown, presented in this thesis. The conclusion is based on the rationale that lithography-based technology would allow seamless integration of a nanopore with electronic and optical sensing circuitry in a precise, efficient and cost effective manner. When we acquire the technology to fabricate such complex and integrated nanopore devices, the degree of freedom in terms of design

will be greatly extended. This renders the potential applications of future nanopore devices way beyond foreseeable projection, which is bounded by current understanding, design and imagination. In the meantime, new simple methods to fabricate small nanopores will accelerate vital researches in the field in preparation for the future of novel technologies.

References

(1) Coulter, W. H. High Speed Automatic Blood Cell Counter and Cell Size Analyzer. *Proc. Natl. Electron. Conf.* **1956**, *12*, 1034–1040.

(2) Rhee, M.; Burns, M. a. Nanopore Sequencing Technology: Nanopore Preparations. *Trends Biotechnol.* **2007**, *25*, 174–181.

(3) Robert Louis Fleischer, Paul Buford Price, R. M. W. *Nuclear Tracks in Solids: Principles and Applications*; University of California Press, 1975; p. 569.

(4) DeBlois, R. W. Counting and Sizing of Submicron Particles by the Resistive Pulse Technique. *Rev. Sci. Instrum.* **1970**, *41*, 909.

(5) Hamill, O. P.; Marty, A.; Neher, E.; Sakmann, B.; Sigworth, F. J. Improved Patch-Clamp Techniques for High-Resolution Current Recording from Cells and Cell-Free Membrane Patches. *Pflügers Arch. Eur. J. Physiol.* **1981**, *391*, 85–100.

(6) Nobelprize.org. The Nobel Prize in Physiology or Medicine 1963 http://www.nobelprize.org/nobel_prizes/medicine/laureates/1963/ (accessed Dec 11, 2014).

(7) Nobelprize.org. The Nobel Prize in Physiology or Medicine 1981 http://www.nobelprize.org/nobel_prizes/medicine/laureates/1981/ (accessed Dec 11, 2014).

(8) Nobelprize.org. The Nobel Prize in Physiology or Medicine 1991 http://www.nobelprize.org/nobel_prizes/medicine/laureates/1991/ (accessed Dec 11, 2014).

(9) Stoddart, D.; Heron, A. J.; Mikhailova, E.; Maglia, G.; Bayley, H. Single-Nucleotide Discrimination in Immobilized DNA Oligonucleotides with a Biological Nanopore. *Proc. Natl. Acad. Sci. U. S. A.* **2009**, *106*, 7702–7707.

(10) Purnell, R. F.; Mehta, K. K.; Schmidt, J. J. Nucleotide Identification and Orientation Discrimination of DNA Homopolymers Immobilized in a Protein Nanopore. *Nano Lett.* **2008**, *8*, 3029–3034.

(11) Manrao, E. a; Derrington, I. M.; Laszlo, A. H.; Langford, K. W.; Hopper, M. K.; Gillgren, N.; Pavlenok, M.; Niederweis, M.; Gundlach, J. H. Reading DNA at Single-Nucleotide Resolution with a Mutant MspA Nanopore and phi29 DNA Polymerase. *Nat. Biotechnol.* **2012**, *30*, 349–353.

(12) Song, L.; Hobaugh, M. R.; Shustak, C.; Cheley, S.; Bayley, H.; Gouaux, J. E. Structure of Staphylococcal Alpha-Hemolysin, a Heptameric Transmembrane Pore. *Science (New York, N.Y.)*, 1996, *274*, 1859–1866.

(13) ZOLLER, M. J.; SMITH, M. Oligonucleotide-Directed Mutagenesis: A Simple Method Using Two Oligonucleotide Primers and a Single-Stranded DNA Template. *DNA* **1984**, *3*, 479–488.

(14) Stoddart, D.; Maglia, G.; Mikhailova, E.; Heron, A.; Bayley, H. Multiple Base-Recognition Sites in a Biological Nanopore: Two Heads Are Better than One. *Angew. Chemie* **2010**, *122*, 566–569.

(15) Kim, M. J.; McNally, B.; Murata, K.; Meller, A. Characteristics of Solid-State Nanometre Pores Fabricated Using a Transmission Electron Microscope. *Nanotechnology* **2007**, *18*, 205302.

(16) Li, J.; Stein, D.; McMullan, C.; Branton, D.; Aziz, M. J.; Golovchenko, J. a. Ion-Beam Sculpting at Nanometre Length Scales. *Nature* **2001**, *412*, 166–169.

(17) Cai, Q.; Ledden, B.; Krueger, E.; Golovchenko, J. a; Li, J. Nanopore Sculpting with Noble Gas Ions. *J. Appl. Phys.* **2006**, *100*, 24914–249146.

(18) Lo, C. J.; Aref, T.; Bezryadin, A. Fabrication of Symmetric Sub-5 Nm Nanopores Using Focused Ion and Electron Beams. *Nanotechnology* **2006**, *17*, 3264–3267.

(19) Storm, a J.; Chen, J. H.; Ling, X. S.; Zandbergen, H. W.; Dekker, C. Fabrication of Solid-State Nanopores with Single-Nanometre Precision. *Nat. Mater.* **2003**, *2*, 537–540.

(20) Aleskovskii, V. Chemistry and Technology of Solids. *J. Appl. Chem. Ussr* **1974**, *47*, 2207–2217.

(21) Chen, P.; Mitsui, T.; Farmer, D. B.; Golovchenko, J.; Gordon, R. G.; Branton, D. Atomic Layer Deposition to Fine-Tune the Surface Properties and Diameters of Fabricated Nanopores. *Nano Lett.* **2004**, *4*, 1333–1337.

(22) Amir G. Ahmadi; Peng, Z.; Nair, S. Wafer-Scale Process for Fabricating Arrays of Nanopore Devices. *J. Micro/Nanolithography, MEMS, MOEMS* **2010**, *9*, 033011.

(23) Merchant, C. a; Healy, K.; Wanunu, M.; Ray, V.; Peterman, N.; Bartel, J.; Fischbein, M. D.; Venta, K.; Luo, Z.; Johnson, a T. C.; *et al.* DNA Translocation through Graphene Nanopores. *Nano Lett.* **2010**, *10*, 2915–2921.

(24) Schneider, G. F.; Kowalczyk, S. W.; Calado, V. E.; Pandraud, G.; Zandbergen, H. W.; Vandersypen, L. M. K.; Dekker, C. DNA Translocation through Graphene Nanopores. *Nano Lett.* **2010**, *10*, 3163–3167.

(25) Uram, J. D.; Ke, K.; Mayer, M. Noise and Bandwidth of Current Recordings from Submicrometer Pores and Nanopores. *ACS Nano* **2008**, *2*, 857–872.

(26) Tabard-Cossa, V.; Trivedi, D.; Wiggin, M.; Jetha, N. N.; Marziali, A. Noise Analysis and Reduction in Solid-State Nanopores. *Nanotechnology* **2007**, *18*, 305505.

(27) Tabard-cossa, V. Instrumentation for Low-Noise High-Bandwidth Nanopore Recording 3. **2013**, 59–93.

(28) Smeets, R. M. M.; Keyser, U. F.; Dekker, N. H.; Dekker, C. Noise in Solid-State Nanopores. *Proc. Natl. Acad. Sci. U. S. A.* **2008**, *105*, 417–421.

(29) Janssen, X. J. a; Jonsson, M. P.; Plesa, C.; Soni, G. V; Dekker, C.; Dekker, N. H. Rapid Manufacturing of Low-Noise Membranes for Nanopore Sensors by Trans-Chip Illumination Lithography. *Nanotechnology* **2012**, *23*, 475302.

(30) Rosenstein, J. K.; Wanunu, M.; Merchant, C. a; Drndic, M.; Shepard, K. L. Integrated Nanopore Sensing Platform with Sub-Microsecond Temporal Resolution. *Nat. Methods* **2012**, *9*, 487–492.

(31) Yusko, E. C.; Johnson, J. M.; Majd, S.; Prangkio, P.; Rollings, R. C.; Li, J.; Yang, J.; Mayer, M. Controlling Protein Translocation through Nanopores with Bio-Inspired Fluid Walls. *Nat. Nanotechnol.* **2011**, *6*, 253–260.

(32) Traversi, F.; Raillon, C.; Benameur, S. M.; Liu, K.; Khlybov, S.; Tosun, M.; Krasnozhon, D.; Kis, a; Radenovic, a. Detecting the Translocation of DNA through a Nanopore Using Graphene Nanoribbons. *Nat. Nanotechnol.* **2013**, *8*, 939–945.

(33) Liu, L.; Yang, C.; Zhao, K.; Li, J.; Wu, H.-C. Ultrashort Single-Walled Carbon Nanotubes in a Lipid Bilayer as a New Nanopore Sensor. *Nat. Commun.* **2013**, *4*, 2989.

(34) Klingfus, J.; Nadzeyka, A.; Bauerdick, S.; Albrecht, T.; Edel, J. B.; Gmbh, R. Wafer-Scale Ion Beam Lithography of Nanopore Devices. *Microsc. Microanal.* **2013**, *19*, 912–913.

(35) Junesch, J.; Sannomiya, T. Ultrathin Suspended Nanopores with Surface Plasmon Resonance Fabricated by Combined Colloidal Lithography and Film Transfer. *ACS Appl. Mater. Interfaces* **2014**, *6*, 6322–6331.

(36) Leibson, S. *Designing SOCs with Configured Cores: Unleashing the Tensilica Xtensa and Diamond Cores*; Morgan Kaufmann Publishers, 2006; p. 16.

(37) Moore, G. E.; Fellow, L. Cramming More Components onto Integrated Circuits. *Proc. IEEE* **1998**, *86*, 82–85.

(38) Gates, B. D.; Whitesides, G. M. Replication of Vertical Features Smaller than 2 Nm by Soft Lithography. *J. Am. Chem. Soc.* **2003**, *125*, 14986–14987.

(39) Austin, M. D.; Ge, H.; Wu, W.; Li, M.; Yu, Z.; Wasserman, D.; Lyon, S. a.; Chou, S. Y. Fabrication of 5 Nm Linewidth and 14 Nm Pitch Features by Nanoimprint Lithography. *Appl. Phys. Lett.* **2004**, *84*, 5299.

(40) Pavel, E.; Jinga, S.; Andronescu, E.; Vasile, B. S.; Kada, G.; Sasahara, a.; Tosa, N.; Matei, a.; Dinescu, M.; Dinescu, a.; *et al.* 2 Nm Quantum Optical Lithography. *Opt. Commun.* **2013**, *291*, 259–263.

(41) Pavel, E.; Jinga, S. I.; Vasile, B. S.; Dinescu, a.; Marinescu, V.; Trusca, R.; Tosa, N. Quantum Optical Lithography from 1nm Resolution to Pattern Transfer on Silicon Wafer. *Opt. Laser Technol.* **2014**, *60*, 80–84.

Chapter 2

Theoretical Framework of Nanofluidic System and Dielectric Breakdown

2.1 Electrical double layer

Liquid bodies in any microfluidic system are bounded by either a solid or a gel interface. These interfaces can sometimes have dominating effects, and their physical behaviors are often unique and complex. For this reason, they are subjected to active researches in the field of interfacial science. In the case of nanopore microfluidic system, both analytes and nanopores are small, and so their interaction with the liquid can be relatively strong. In particular, it is known that ionic concentration near a solid-liquid interface can be deviated from the bulk concentration, forming what is known as an electrical double layer (EDL). The presence of an EDL can have a determinate effect on the flow profile and conductance of a nanopore. For this reason, the following sections outline the theoretical framework related to EDL and nanopore fluidic system.

2.1.1 Origin of Electrical Double Layer

Electrical double layer is a theoretical concept to model ion distribution close to a solid-electrolyte interface. A solid surface submerged in liquid electrolyte can cause perturbation of ion concentration at its vicinity. Physical origins of the perturbation are ion absorption, protonation/deprotonation, and external electrical potential. These mechanisms work in conjunction with diffusion (osmotic pressure) to construct a continuous ion concentration profile, extending to the bulk liquid body. The double layer refers to the Stern layer, where chemical interaction takes place, and a Gouy-Chapman layer, where ions concentration profile is governed by diffusion[1–3], as illustrated in figure 2.1. The Stern layer can be further divided into inner and outer Helmholtz layers considering finite size of the ions and their hydration shell respectively.

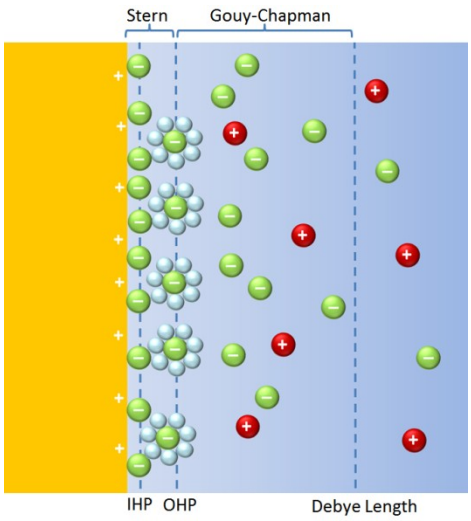

Figure 2.1: Illustration of the electrical double layer of a positively charged surface. Dash lines illustrated where the inner Helmholtz plane (IHP), outer Helmholtz plane (OHP) and the Gouy-Chapman diffusive layer are defined. Outer Helmholtz layer arises because of the existence of a hydration shell surrounding some counterions.

2.1.2 Poisson-Boltzmann Model

At equilibrium, chemical potential at a surface is balanced by the electrical potential of the ions profile. Under electrostatic condition, electrical potential, ψ, is related to the volume charge density, ρ, by the Poisson equation:

$$\nabla^2\psi = -\frac{\rho}{\varepsilon}, \tag{2.1}$$

where ε is the permittivity of the medium. Consider an ion specie with (number) concentration, n_i and charge valence, z_i, being perturbed by a potential to deviate from the bulk concentration, n_i^{∞}. The system would follow the Boltzmann statistic, thus:

$$n_i = n_i^{\infty} exp\left(-\frac{z_i e\psi}{kT}\right). \tag{2.2}$$

In an electrolyte solution, the charge density is a sum of charge contribution from all ions species:

$$\rho = \sum_i z_i e n_i, \tag{2.3}$$

where *e* is the elementary charge. Combining Eqs 2.1, 2.2, and 2.3 yield the *Poisson-Boltzmann* Equation[2,4,5]:

$$\nabla^2\psi = -\frac{e}{\varepsilon}\sum_i z_i n_i^{\infty} exp\left(-\frac{z_i e\psi}{kT}\right). \tag{2.4}$$

This equation is a second order ordinary differential equation, and leads to a boundary condition problem. On a planar surface, it has an analytical solution, but most often it is solved numerically on other geometries.

2.1.3 Debye-Huckel Approximation

Debye-Huckel model concern the scenario when ion concentration is low. At this condition, $z_i e\psi \ll kT$, the exponential term can be expanded into Maclaurin series and approximated to the second order as:

$$exp\left(-\frac{z_i e\psi}{kT}\right) = \sum_{j=0}^{\infty}\left(-\frac{z_i e\psi}{kT}\right)^j / j! \approx 1 - \frac{z_i e\psi}{kT}. \tag{2.5}$$

Substitute this approximation into the *Poisson-Boltzmann* equation Eq 2.4 yields:

$$\nabla^2\psi = -\frac{e}{\varepsilon}\sum_i z_i n_i^{\infty}\left(1 - \frac{z_i e\psi}{kT}\right). \tag{2.6}$$

The first term inside summation is zero considering net charge neutrality of the bulk, which gives a linearized version of *Poisson-Boltzmann* equation:

$$\nabla^2\psi = \frac{e^2}{\varepsilon kT}\sum_i z_i^2 n_i^{\infty}\psi = \kappa^2\psi, \tag{2.7}$$

where κ is known as the Debye–Hückel parameter and its inverse is the Debye length, λ. Rewritten in molar concentration, c_i (in SI unit of mM), the Debye length is

$$\lambda_D = \kappa^{-1} = \left[\frac{e^2 N_A}{\varepsilon kT}\sum_i z_i^2 c_i^{\infty}\right]^{-\frac{1}{2}}. \quad (2.8)$$

This length scale characterizes the range at which effect of counterions cannot be ignored. Although the derivation of Debye length begins with low salt approximation, this characteristic length scale is applicable to high salt condition to a rough estimate. In a 1M monovalent salt, Debye length is about 3Å. According to Eq 2.8, multivalent ions can reduce the Debye length by a fraction. This effect is important to kinematics of long polymers chains.

2.1.4 Gouy-Chapman Model

Gouy-Chapman equation[6,7] provides an accurate description for both high and low salt concentrations. It is an analytical solution to the *Poisson-Boltzmann* equation. Consider the scenario of a planar surface submerged in liquid, Eq 2.4 can be reduced to a first order ordinary differential equation through the method of integrating factor multiplication, which yields:

$$\left(\frac{d\psi}{dx}\right)^2 = \frac{2kT}{\varepsilon}\sum_i n_i^{\infty} exp\left(-\frac{z_i e\psi}{kT}\right) + C_1, \quad (2.9)$$

where, C_1 is an integration constant. It can be obtained by considering that both ψ and $\frac{d\psi}{dx}$ reach zero when x approach infinity, which gives:

$$C_1 = -\frac{2kT}{\varepsilon}\sum_i n_i^{\infty}, \quad (2.10)$$

thus, Eq 2.9 becomes:

$$\left(\frac{d\psi}{dx}\right)^2 = \frac{2kT}{\varepsilon}\sum_i \left[n_i^{\infty} exp\left(-\frac{z_i e\psi}{kT}\right) - 1\right]. \quad (2.11)$$

Consider a two ions system where cation and anion are symmetric in valance, for instance, $z_i = \pm z$, then Eq 2.11 can be further simplified to:

$$\left(\frac{d\psi}{dx}\right)^2 = \frac{2kTn^{\infty}}{\varepsilon}\left[exp\left(-\frac{ze\psi}{2kT}\right) - exp\left(\frac{ze\psi}{2kT}\right)\right]^2, \quad (2.12)$$

which can be solved analytically and yield:

$$ln\left[\tanh\left(\frac{ze\psi}{4kT}\right)\right] = -\kappa x + C_2. \quad (2.13)$$

The integration constant, C_2, is evaluated by considering that diffusive mechanism is valid up to the Stern layer interface, at which it is *d* away from the surface, and has a Stern potential of ψ_d. This gives:

$$C_2 = ln\left[\tanh\left(\frac{ze\psi_d}{4kT}\right)\right] + \kappa d, \quad (2.14)$$

and Eq 2.13 becomes:

$$\tanh\left(\frac{ze\psi}{4kT}\right) = \tanh\left(\frac{ze\psi_d}{4kT}\right)\exp\left[-\kappa(x-d)\right]. \quad (2.15)$$

This equation is known as the Gouy-Chapman equation, which describes the ionic profile at the diffusive layer. Although this equation is referenced with respect to the Stern layer interface, other reference point can be inflicted. In practical consideration, zeta potential is more commonly accessible and sometimes the only parameter available. The equation can give an equivalent solution using the zeta potential defined at the hydrodynamic slip plane and the corresponding distance as input parameter.

2.1.5 Grahame Model

Grahame model[1] concerns the charge density at the Stern layer. For planar surface, it can be derived directly from the solution of Gouy-Chapman model. Consider bulk electroneutrality, the net surface charge density on the Stern layer, ρ_d, must be equal and opposite to the net charge (per area) of the diffusive layer. Evaluation of the relation with Gauss's law yields:

$$\rho_d = -\int_d^\infty \rho dx = -\varepsilon \frac{d\psi}{dx}\Big|_{x=d}. \tag{2.16}$$

Substitute Eq 2.12 into Eq 2.16 and evaluate at $x = d$ gives[1]:

$$\rho_d = \sqrt{2\varepsilon kTn^\infty}\left[exp\left(\frac{ze\psi_d}{2kT}\right) - exp\left(-\frac{ze\psi_d}{2kT}\right)\right], \tag{2.17}$$

which can be rewritten as[1]:

$$\rho_d = \sqrt{8\varepsilon kTn^\infty}\sinh\left(\frac{ze\psi_d}{2kT}\right). \tag{2.18}$$

This is known as the Grahame equation, which relates the Stern potential to the surface charge density at the Stern layer. The surface charge density plays an important role in pseudocapacitance, charge transfer, surface conductance, electrochemical reaction and many other electrokinetic phenomena.

2.2 Electroosmosis in a Nanopore

Electroosmotic flow (EOF) is an induced liquid motion caused by an applied electric field. It is caused by an unbalanced net Coulomb force from cations and anions. The effect is induced at the presence of an electrical double layer, where one ionic charge dominates over the other, and the local net charge density is not zero. It is most pronounced when a surface is parallel to the electric

field. When a liquid body is surrounded by a surface, as in the case of a capillary or tube, EOF induced at the wall motivate the bulk liquid body to flow. When a long fluidic channel has a uniform width along its axis, motion is induced uniformly at the surrounding wall. At this scenario, there is no differential pressure away from the wall, and the bulk liquid body flows with a planar flow profile, as if the bulk is being carried by the liquid close to the wall. This is known as a plug flow, and has a no shear component in velocity field away from the wall. It is important to note that this plug flow picture is only applicable to fluidic channels with high aspect ratio, in which the length is much larger than the width of the channel so that the edge effects from the entrance and exit are negligible. However, in a nanopore, this is often not the case. In fact, edge effect from the openings is important to the flow profile of most nanopore systems.

EOF is an electrokinetic phenomenon coupled with fluid dynamic. When a hydrodynamic plug flow assumption is not applicable, finite element (FE) numerical analysis is often the choice for studying such problem. FE analysis requires the input of a correct microscopic physical model in order to simulate the macroscopic properties of the system. Under an external voltage bias, equilibrium description of ionic profile, as in the Poisson equation, is insufficient because mass transport must also be considered. In this case, Nernst-Planck equation is more accurate in describing the physics in the system. It relates the mass transport of ions flux to the ionic concentration gradient and electric field, which states that the ion fluxes[8],

$$J_i = -D_i \nabla c_i + \frac{z_i e c_i}{kT} \nabla \psi, \tag{2.19}$$

where D_i is the diffusivity of the *i-th* specie. This equation works in conjunction with the Poisson equation, Eq 2.1, to form the basis of the Poisson-Nernst-Planck (PNP) model[9]. In steady state,

$$\nabla \cdot J_i = 0. \tag{2.20}$$

Fluid dynamic is introduced with the Stokes divergence equation [8]:

$$-\nabla p + \gamma \Delta \vec{u} - e\nabla\psi \sum_i z_i\, c_i. \tag{2.21}$$

Numerous studies based on the PNP model showed some interesting results. Paik *et al.*[8] considered a gated nanopore, which has an embedded metalized layer inside a dielectric membrane. His simulation shows that EOF can be made to work against the electrophoretic capturing of DNA molecules. And by adjusting the strength of EOF, the nanopore device can be electrically controlled to accept or reject DNA. This is functionally equivalent to a DNA transistor in a nanofluidic system.

2.3 Nanopore Conductance Models

2.3.1 Nanopore Conductance at High Concentration

Nanopore conductance models are crucial for any pulse-resistive-based applications. All pulse-resistive methods require the knowledge of the relationship between the open-pore conductance and the nanopore geometry, and to relate these to extract analytes information from the blocked-pore conductance. At high ion concentration regime, the Debye length is small relative to the radius of most nanopores. Consider 1M monovalent salt electrolyte solution, which is very common in nanopore electrophoretic experiment, the Debye length is around a few Angstroms according to Eq 2.8, which is much less than the diameter of a typical nanopore. In this scenario, surface conductance can be ignored, and a nanopore has a conductance[10],

$$G(d) = \sigma \left[\frac{4l}{\pi d^2} + \frac{1}{d}\right]^{-1}, \tag{2.22}$$

where σ is the bulk conductivity, l and d is the effective length and diameter of a pore. The second term inside the equation originated from the access resistance of the pore opening. The magnitude of the access resistance is increasingly dominating as the diameter increase. This partly contributes to the fact that small nanopore has better sensitivity for resistive-pulse experiment. This also explains why the capability to precisely fabricate nanopore around 1.5nm diameter is crucial for DNA sensing or sequencing applications. It is important to note from Eq 2.22 that a nanopore system also approaches access resistance domination when $l \to 0$. This is the monolayer limit, like a graphene nanopore system, at which resistance is concentrated at the rim outside the pore opening. There are reports showing that access resistance scales with d^{-2} at this limit instead[11], implying that the equation is not applicable at this limit.

When a DNA molecule is electrophoretically driven through a nanopore, the physical blockage of ionic current can causes a discrete drop in conductance. This is the fundamental mechanism of resistive-pulse sensing mechanism. The drop in conductance can be modeled according to Eq 2.22, considering that [10]:

$$\Delta G = G(d) - G(d'_D), \tag{2.23}$$

where d'_D is the effective diameter of a pore at the presence of a DNA molecule. It is defined in this model as $d'_D = \sqrt{d^2 - d_{DNA}^2}$, and d_{DNA} is the diameter of a DNA molecule, taken as 2.2nm for dsDNA and 1.4nm for ssDNA.

2.3.2 Conductance at low salt concentration

At low concentration, surface conductivity from EDL cannot be ignored. Ralph *et al.* developed a model considering surface conduction[12]. His model stated that the conductance of a nanopore is:

$$G(d) = \frac{\pi}{4l}(\sigma d^2 + 4\rho_s \mu_c d), \tag{2.23}$$

where ρ_s is the surface charge density and μ_c is the electrophoretic mobility of the surface charge carrier at the diffusive layer. According to the Grahame model, Eq 2.18, the surface charge density at the hydrodynamic slip-plane where the zeta potential, ζ, is defined, is:

$$\rho_s = \sqrt{8\varepsilon kTn^{\infty}} \sinh\left(\frac{e\zeta}{2kT}\right), \tag{2.24}$$

or rewritten according to Eq 2.8 as:

$$\rho_s = \frac{2\varepsilon kT}{e\lambda_D} \sinh\left(\frac{e\zeta}{2kT}\right), \tag{2.25}$$

for monovalent electrolyte solution.

At low salt concentration, conductivity of counter-ions surrounding an electrophoretically driven molecule can be comparable to the solution. For this reason, change in conductance when a DNA pass-through must also consider the effective conductivity of the counter-ion cloud. According to Eq 2.23, it has the form[12]:

$$\Delta G = \frac{-\pi\sigma d_{DNA}^2}{4l} + \frac{\mu_c^* q_{DNA}^*}{l}, \tag{2.26}$$

where μ_c^* is the effective electrophoretic mobility of the counter ions of DNA molecule, while q_{DNA}^* is the linear charge density of the DNA. In this equation, the conductivity of the counter-ions brought by a DNA molecule can act opposite to the effect of current blockage. When the two

terms balanced each other, $\Delta G = 0$, and a nanopore cannot detect a DNA molecule through resistive-pulse sensing mechanism.

2.4 Percolation theory of dielectric breakdown

In the course of developing models for time dependent dielectric breakdown (TDDB), two independent suggestions were proposed. The first is known as a critical electron trap density (CETD) model[13–15]. Electron traps are localized electronic structure defects in a dielectric material. It manifests as intermediate energy levels in a band gap between the valance band and the conduction band. These levels are otherwise forbidden without the presence of defects. They can be generated with thermal stress or electric field stress. Because they have lower energy level than the conduction bands, electrons (or holes equivalently for hole trap) will more readily fill them upon excitation. And because these defects are localized and isolated in coordinate space, it is a trap, physically confining an electron. Lastly, the presence of theses intermediate energy levels lower the energy barrier for electron tunneling, which can facilitate what is known as trap assisted tunneling current (TAT)[16–18], at which electrons can hop between these traps. CETD suggests that TDDB occurs when a critical number of trap is generated. On the other hand, a second school of thought claims that TDDB occurs when a critical hole fluence is reached[19]. Hole fluence is the total flux of holes (sum over time). It is generated through a process called anode hole injection (AHI)[18]. When an energetic electron driven by a field reaches the anode, it can exchange its energy with an electron deep in the valance band, and promotes it to the conduction band edge. As a result, a hot hole is created. Experimentally, it is shown that there exists critical values of hole fluence at which TDDB occur[19].

Given the competition between the two schools of thought, of which both have good experimental evidences to support, Degraeve *et al.* provided a new insight that reconciled both sides[20]. His theory is known as the percolation theory. The theory explains that TDDB is correlated to CETD because electron traps can form a conductive path between anode and cathode upon reaching a critical value, at which dielectric breakdown occurs. Then, he illustrated experimentally that the generation of electron trap is strongly correlated with the generation of hole fluence. The empirical relationship he found was [20]:

$$D_T = cQ_p^{0.56}, \tag{2.27}$$

where D_T is the total electron trap density, Q_p is the hole fluence, and c is a numerical constant inversely proportional to the fraction of electron trap filled with an electron. For this reason, critical condition for both hole fluence and electron traps are equivalent in nature. This model provides good agreement with experimental data and is widely accepted as a good model.

The model describes several interesting properties relevant to the control of dielectric breakdown. Firstly, the TDDB is independent of the degradation mechanism, neither Fowler–Nordheim (FN) tunneling at high field nor substrate hot electron (SHE) tunneling at medium field. Secondly, the occurrence of a TDDB is a weakest link problem, and so it follows Weibull statistics. Thirdly, a thin membrane requires less electron traps to complete a path and will have a dielectric breakdown with less stress. However, the time variance for such event increases.

References

(1) Grahame, D. C. The Electrical Double Layer and the Theory of Electrocapillarity. *Chem. Rev.* **1947**, *41*, 441–501.

(2) Ghosh, P. Electrostatic Double Layer Force: Part II.

(3) SMIRNOV, S. N. Electric Double Layer http://web.nmsu.edu/~snsm/classes/chem435/Lab14/double_layer.html (accessed Dec 10, 2014).

(4) Fogolari, F.; Brigo, a; Molinari, H. The Poisson-Boltzmann Equation for Biomolecular Electrostatics: A Tool for Structural Biology. *J. Mol. Recognit.* **2002**, *15*, 377–392.

(5) Poisson-Boltzmann equation http://en.wikipedia.org/wiki/Poisson-Boltzmann_equation (accessed Dec 10, 2014).

(6) Gouy, M. Sur La Constitution de La Charge Électrique À La Surface D'un Électrolyte. *J. Theor. Appl. Phys.* **1910**, *9*, 457–468.

(7) Chapman, D. A Contribution to the Theory of Electrocapillarity. *Philos. Mag.* **1913**, *25*, 475–481.

(8) Paik, K.; Liu, Y.; Tabard-Cossa, V.; Waugh, M. J.; Huber, D. E.; Provine, J.; Howe, R. T.; Dutton, R. W.; Davis, R. W. Control of DNA Capture by Nanofluidic Transistors. *ACS Nano* **2012**, *6*, 6767–6775.

(9) Lu, B.; Zhou, Y. C. Poisson-Nernst-Planck Equations for Simulating Biomolecular Diffusion-Reaction Processes II: Size Effects on Ionic Distributions and Diffusion-Reaction Rates. *Biophys. J.* **2011**, *100*, 2475–2485.

(10) Kowalczyk, S. W.; Grosberg, A. Y.; Rabin, Y.; Dekker, C. Modeling the Conductance and DNA Blockade of Solid-State Nanopores. *Nanotechnology* **2011**, *22*, 315101.

(11) Schneider, G. F.; Kowalczyk, S. W.; Calado, V. E.; Pandraud, G.; Zandbergen, H. W.; Vandersypen, L. M. K.; Dekker, C. DNA Translocation through Graphene Nanopores. *Nano Lett.* **2010**, *10*, 3163–3167.

(12) Ralph, M.; Smeets, M.; Keyser, U.; Krapf, D. Salt Dependence of Ion Transport and DNA Translocation through Solid-State Nanopores. *Nano Lett.* **2006**, *6*, 89–95.

(13) Schuegraf, K.; Hu, C. Effects of Temperature and Defects on Breakdown Lifetime of Thin SiO2 at Very Low Voltages. *Electron Devices, IEEE Trans.* **1994**, *41*, 1227–1232.

(14) Schuegraf, K. F.; Hu, C. Metal-Oxide-Semiconductor Field-Effect-Transistor Substrate Current during Fowler–Nordheim Tunneling Stress and Silicon Dioxide Reliability. *J. Appl. Phys.* **1994**, *76*, 3695.

(15) Chen, I. C.; Holland, S.; Young, K. K.; Chang, C.; Hu, C. Substrate Hole Current and Oxide Breakdown. *Appl. Phys. Lett.* **1986**, *49*, 669.

(16) Nasyrov, K. a.; Shaimeev, S. S.; Gritsenko, V. a. Trap-Assisted Tunneling Hole Injection in SiO2: Experiment and Theory. *J. Exp. Theor. Phys.* **2009**, *109*, 786–793.

(17) Wut, J.; Register, L. F.; Rosenbaumt, E. Trap- Assisted Tunneling Current Through Ultra-Thin Oxide. **1999**, 389–395.

(18) DiMaria, D. J.; Cartier, E.; Buchanan, D. a. Anode Hole Injection and Trapping in Silicon Dioxide. *J. Appl. Phys.* **1996**, *80*, 304.

(19) Schuegraf, K.; Hu, C. Hole Injection SiO2 Breakdown Model for Very Low Voltage Lifetime Extrapolation. *Electron Devices, IEEE Trans.* **1994**, *41*, 761–767.

(20) Degraeve, R.; Groeseneken, G. New Insights in the Relation between Electron Trap Generation and the Statistical Properties of Oxide Breakdown. *Electron Devices, ...* **1998**, *45*, 904–911.

Chapter 3

Signal Processing and Digital Filter: Theory and Implementation

3.1 Overview of Signal Processing and Filters

Noise is a major barrier in nanopore pulse-resistive-sensing applications, especially when the temporal duration of a signal is short or signal-to-noise ratio is low. For this reason, noise filtering is crucial in analysing an ionic current trace from a resistive-pulse sensing experiment. It allows the distinction and recognition of some translocation events, which would otherwise be hidden in the noise. Data from nanopore electrophoretic experiment are typically filtered with an analog filter and a digital filter. Analog filters are built-in to most of the commonly used commercial current amplifiers. For the Axopatch 200B we used, it has a low-pass 4-pole Bessel filter with maximum filtering frequency of 100kHz, while the MultiClamp 700B has a Bessel or Butterworth filter with a maximum filtering frequency of 30kHz. The MultiClamp 700B also has an option to bypass the analog filter. While analog filters in a current amplifier are built-in and standardized, the design of digital filters requires specific knowledge and attention. The digital filter we used was coded in the language of Labview. It employs a zero phase 4^{th}-order Butterworth (IIR) low-pass filter. Detail of this filter is discussed in the following sections.

3.2 FIR and IIR filter

Digital filtering is a mathematical process that operates on a digital time series. It is a linear transformation of an input series, into a corresponding output series. The output series will have a modulated frequency spectrum compared to the input. For electrophoretic resistive-pulse experiment, a current trace would be the time series of interest. Equivalent to an analog filter, digital filters can operate on high-pass, low-pass, band-pass or band-stop filtering mode. Digital filters are divided into two main categories: infinite impulse response (IIR) and finite impulse response (FIR) filters. For IIR filters, a finite impulse input has an output response that extends to

infinity. A useful filter usually has an infinite response that decays, approaching zero. On the contrary, FIR filter has a response that terminates in finite steps. A general form of digital filtering transformation can be expressed as[1]:

$$y[n] = \frac{1}{b_0}\left(\sum_{j=0}^{P} a_j x[n-j] - \sum_{j=1}^{Q} b_j y[n-j]\right) \quad , \tag{3.1}$$

and equivalently,

$$\sum_{j=0}^{Q} b_j y[n-j] = \sum_{j=0}^{P} a_j x[n-j] \quad , \tag{3.2}$$

where $y[n]$ and $x[n]$ are the nth point in the output and input series respectively, P and Q are feedforward and feedbackward order, while a_j and b_j are feedforward and feedbackward coefficients corresponding to the specific filter of choice. The second summation term in Eq 3.1 recursively subtracts previous filtered terms. This is how a response in IIR propagates to infinity beyond P steps. And for this reason, any causal FIR filter, $b_j = 0$ for all $j > 0$.

Consider applying a discrete Fourier transformation (DFT) on both the output and input series with the z-transformation function as the kernel[2–4], namely:

$$X[z] = \sum_n x[n]z^n \quad \text{and} \quad Y[z] = \sum_n y[n]z^n \quad , \tag{3.3}$$

where $z = Ae^{i\omega}$ is a complex number and $X[z]$ and $Y[z]$ are the corresponding series expressed in the frequency domain. Then any filtering transformation can be expressed as:

$$Y[z] = H[z]X[z], \tag{3.3}$$

where $H[z]$ is known as the transformation function. According to Eq 3.2-3.4 [1],

$$H[z] = \sum_{j=0}^{P} a_j z^{-j} \Big/ \sum_{j=0}^{Q} b_j z^{-j} \quad , \tag{3.4}$$

For any FIR, $H[z]$ have a real denominator, while for any IIR, as in the case of a Butterworth filter, the denominator is complex[1].

3.3 Zero Phase Filter and Causality

In practical use of a digital filter for data analysis on resistive-pulse experiment, a filtered series is used to identify discrete pulse events in the input (original) series. For this reason, both series must be in-phase. However, Eq 3.1 is biased forward in *n*. In other words, the n^{th} output only depends on previous input data. This introduces asymmetry in the time domain, and will therefore always have a phase lag between the output and the input series. In addition, the phase lag is dependent on the magnitude of an impulse. This makes post-process compensation difficult. The phase lag is present because causality is enforced. A causal relationship refers to the fact that an output series at *n* cannot be responding to an impulse in the input series at $n + i$, for any $i > 0$ (future events). In order to have the output series in-phase with the input series, both causal relation and time asymmetry must be removed objectively. A simple technique to achieve this zero phase filtering is to apply the transformation function twice; in the forward and backward time direction.

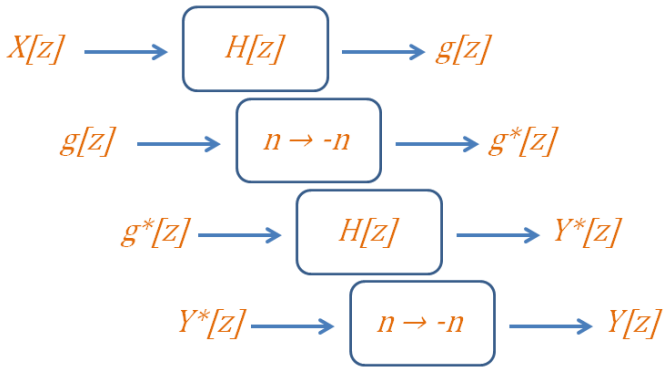

Figure 3.1: Illustration of a zero phase transformation. Time reversal is inflicted between the two transformation operations of *H[z]*, and then it is reverted back at last to the correct time direction. g is an intermediate function.

Applying a transformation function in the forward and backward time direction on a series is equivalent mathematically to inflicting the time reversal transformation between two identical transformation operations, as illustrated in figure 3.1. In DFT, time reversal simply gives a conjugate output. For instance, consider Eq3.3, when $n \rightarrow -n$, then $H[z]X[z] \rightarrow H^*[z]X^*[z]$. With this in mind, it is simple to prove that this time reversal scheme produces a zero phase transformation. Consider that the net effective transformation function is $H'[z]$, then the net transformation as shown in Figure 3.1 can be expressed as:

$$Y[z] = H'[z]X[z], \tag{3.5}$$

which can be rewritten according to the scheme illustrated in figure 3.1 as [5]:

$$Y[z] = H^*[z]H[z]X[z] = |H[z]|^2 X[z] , \tag{3.6}$$

and so $H'[z] = |H[z]|^2$ and is real. This implies that there is not a phase difference between $Y[z]$ and $X[z]$ in the complex space, and so there is no time difference between $y[n]$ and $x[n]$ in temporal space. It is important to note that zero phase filter is non-causual. This implies that the filter cannot operate in a continuous manner.

3.4 Implementation and Practical Consideration

When a zero phase filter is implemented numerically in a computer, there are practical constraints one need to consider. For instance, the transformation requires the knowledge of future events in order to go both forward and backward in time domain. This two-pass transformation scheme prohibits analysis of a time series in a sequential and continuous manner. A typical electrophoretic experiment usually spans several hours. Considering that the data are being digitized at 250kHz, the size of data would be in the range of gigabytes, which is at the limit of random access memory (RAM) available in current personal computers. Operating the transformation on the entire data set would therefore require permanent storage space equal to the original data set. A simple method to by-pass this problem is to operate the transformation in a piece-wise manner, dividing a time series into sub-pieces. This is also known as windowing. However, there is another issue with this method. Consider a sub-piece of the divided data that is between n_1 and n_2 inclusively. For simplicity of the argument, let $P = Q$. Then, according to Eq3.1, computation of $y[n_1]$ would require the knowledge of $x[n_1 - P]$ for any causal FIR filter. Similarly, because zero phase transformation is time reversible, computation of $y[n_2]$ would also require the knowledge of $x[n_2 + P]$. To solve this problem, the sub-piece of a series would be padded by extra data point on both ends. This implies the computation of some overlapped data, which translates to computation overhead and inefficiency. This problem is much more pronounced for IIR filter. Consider again Eq 3.1 for IIR filters, the computation of $y[n_2]$ would require the knowledge of $y[n_2 + P]$, which recursively requires the knowledge of $y[n_2 + 2P]$, $y[n_2 + 3P]$, … , $y[\infty]$. For practical implementation, the padding must cease at some cut-off, and so there must be some trivial data points included in the padding. Figure 3.2 explains how a sub-series is padded to obtain a piece-wise filtered output series. It is important to note that the trivial data added to the two ends of a

series would introduce edge effect (error) to $y[n]$. To minimize the effect, the non-trivial padding length, L, must be much larger than the decaying half-life of an impulse responds.

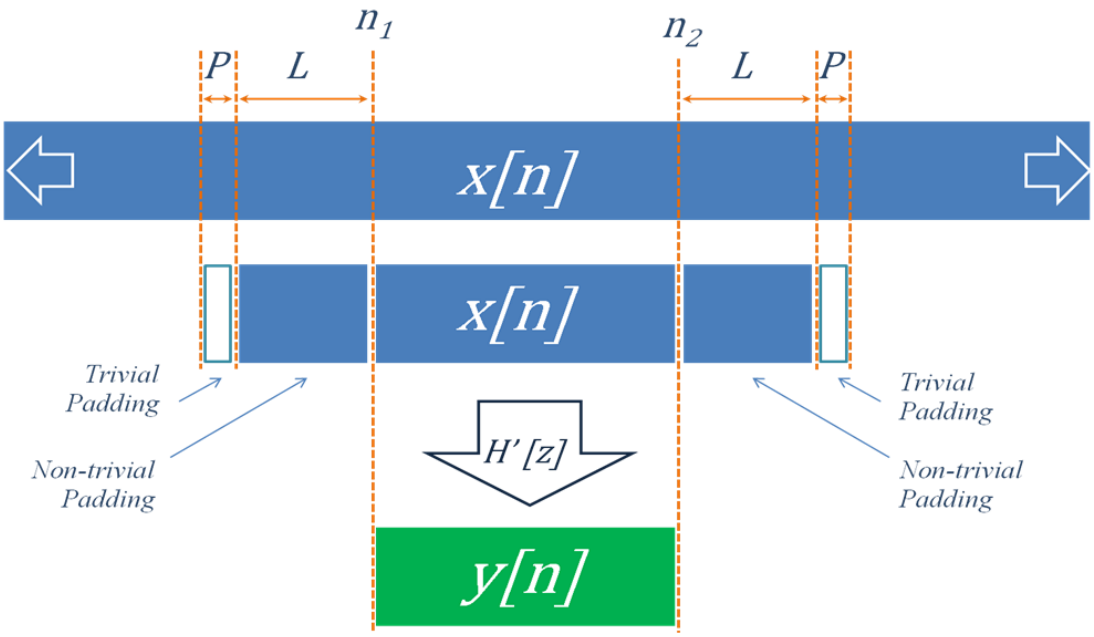

Figure 3.2: Illustration of the method of padding for piece-wise zero phase filtering. A long input series *x[n]* is subdivided into pieces. A particular chunk of interests, between n_1 and n_2, is padded with the additional trivial and non-trivial data in order to obtain an output series between n_1 and n_2. Trivial padding can be a set of zeros or any arbitrary numbers. The trivial padding will cause edge effects, and so L must be large.

References

(1) Infinite impulse response http://en.wikipedia.org/wiki/Infinite_impulse_response (accessed Dec 10, 2014).

(2) Ragazzini, J. R.; Zadeh, L. A. The Analysis of Sampled-Data Systems. *Trans. Am. Inst. Electr. Eng.* **1952**, *71*, 225–234.

(3) Oppenheim, A. V.; Schafer, R. W. *Discrete-Time Signal Processing*; Prentice Hall: Upper Saddle River, N.J, 1999.

(4) Jury, E. I. *Theory and Application of the Z-Transform Method*; Krieger Pub Co, 1973.

(5) Veen, B. Van. Zero Phase Filtering http://allsignalprocessing.com/zero-phase-filtering/.

Chapter 4

Nanopore Fabrication by Controlled Dielectric Breakdown

A related version is published in PLoSOne:
H. Kwok, K. Briggs, and V. Tabard-Cossa, "Nanopore fabrication by controlled dielectric breakdown.," *PLoS One*, vol. 9, no. 3, p. e92880, Jan. 2014.

Abstract

Solid-state nanopores are emerging as versatile single-molecule analytical tools for a host of applications, including DNA sequencing and clinical diagnostic applications. However, the process of fabricating a nanopore is currently a bottleneck to the related field of researches and applications. Current nanopore fabrication techniques rely on dedicated equipments and handling. A rapid and low-cost fabrication method for nanometer-sized solid-state pore represents a breakthrough in the field. Here reports a surprisingly simple method for fabricating individual solid-state nanopore in a thin dielectric membrane. The method relies on driving a tunnelling current across an intact dielectric membrane while immersed in aqueous solution. Current is monitored in real-time to detect the onset of a dielectric event, upon which a small nanopore is created. With this method, it was shown that a pore as small as 1-nm could be fabricated reliably and its size could be subsequently enlarged with sub-nm precision. We found that nanopores fabricated by this process exhibit ohmic behavior and stable conductance over extended periods of time. These pores are capable of detecting translocation events of individual DNA molecule, confirming their usefulness as single-molecule sensors. A discussion on the creation mechanism, control parameters and properties of the resulting nanopores is provided.

4.1 Introduction

Nanotechnology relies on our ability to manipulate matter and fabricate device structure at the nanometer scale. Present solid-state fabrication methods reproducibly achieving dimensional control at the nanometer scale are often complex and involve the use of expensive infrastructure, operated by highly qualified personnel. For instance, the problem of fabricating a molecular-scale hole, or nanopore, in a thin insulating solid-state membrane requires the use of focused high-energy particles, either produced by a dedicated ion beam machine (ion-beam sculpting)[1–3], an irradiation source (Track Etched Membrane)[4], or a transmission electron microscope (TEM drilling)[5]. Although these advances in nanofabrication have placed the fabrication of nanoscale devices with sub-nm control within reach for academic laboratories, they are poorly suited for mass-producing holes into an insulating layer to create pores. This represents a major barrier to the commercialization of any solid-state nanopore-based technologies for health science applications, including rapid DNA sequencing.

Nanopore sensing relies on the electrophoretically driven translocation of biomolecules through nanometer-scale holes embedded in thin insulating membranes to confine, detect and characterize individual biological molecules electrically[6–10]. When a small voltage bias (~100mV) is applied across a nanopore in a membrane separating two chambers of aqueous electrolyte (e.g. 1M KCl), the resulting ionic current through the pore can be measured with a standard current amplifier. As a molecule is driven through a pore, the resulting reduction or fluctuation of ionic current indicates the presence of the molecule and can provide structural information (i.e. the molecule's length, size, conformation, and composition)[11]. A proteinaceous pore (alpha-Hemolysin) was first used to detect ssDNA in 1996 [12]. Since that time, a host of applications for nucleic acid and protein analysis using

both biological and solid-state nanopores have been developed [13]. Compared to their organic counterparts, solid-state nanopores are an essential component of a practical nanopore-based instrumentation due to their increased durability, size and shape control, and their natural propensity for integration with wafer scale technologies (MEMS, CMOS)[14]. Yet, those nanopore fabrication methods used routinely in today's research environment cannot be employed for the commercialization of solid-state nanopore-based technologies due to high-cost and related scale up issues. In this chapter, we introduce an alternative fabrication method that is scalable, simple and low-cost, allowing nanopores to be created directly in aqueous solution, which greatly facilitates storage, handling and use.

4.2 Results and Discussion

4.2.1 Nature of tunneling current and mechanism leading to a dielectric breakdown event

Individual nanopores were created on thin insulating solid-state membranes directly in solution. A thin silicon nitride (SiN_x) membrane, supported by a silicon frame, is mounted in a liquid cell and separates two liquid reservoirs. The reservoirs are first filled with 95% ethanol to remove any air bubbles, followed by slowly replacing it with di-ionized water and then 1M KCl solution. Prior cleaning of the membrane is not necessary. This is contrary to nanopore created in ambient environment, which requires treating the SiN_x surface with acid or plasma to reduce the hydrophoblicity for wetting purpose. Ag/AgCl electrodes immersed on both sides of the membrane are connected to a custom-built resistive feedback current amplifier, as shown in figure 4.1a, which can apply a potentials bias of up to ±20V across a membrane. The setup shown in Figure 4.1b is otherwise identical to setup commonly employed for molecular sensing experiments. This

immensely improved practicality by eliminating tedious and unnecessary remounting and wetting protocols.

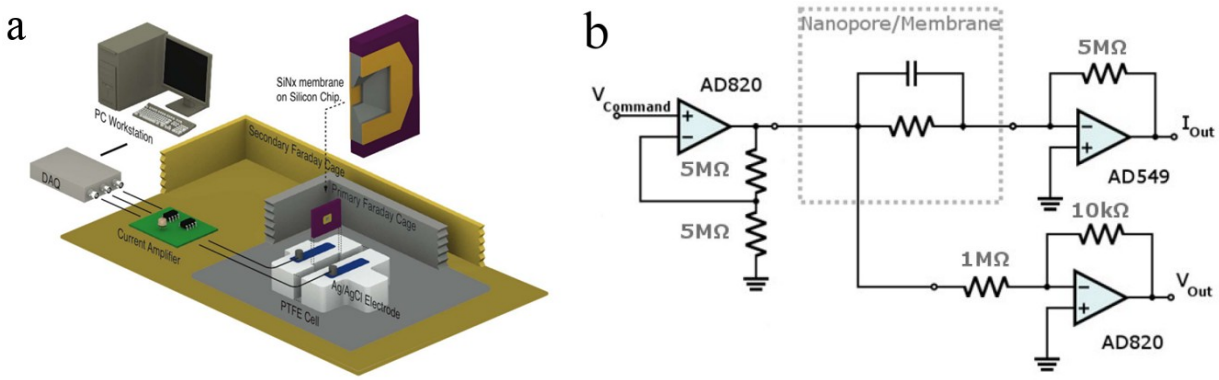

Figure 4.1: Experimental setups. a) Schematic of the experimental setup used to fabricate nanopores directly in aqueous solutions. b) Schematic of the custom current amplifier. Op-amps are powered with 20V source.

Pristine dielectric membranes allow leakage current to pass through when they are subjected to a relatively high external electric field. This current is referred to as stress induced leakage current (SILC)[15–18]. Figure 4.2a illustrated some typical leakage current level of the SiN_x membranes at different electric field strength. These currents are not ionic in nature, and are not related to pin holes or pre-existed nanopores. During the fabrication process, both current and voltage are monitored in real time. Figure 4.2b illustrated a current and a voltage trace of a fabrication experiment on a 10nm SiN_x membrane. A constant potential bias of 5V is applied across the membrane. The corresponding electric field is ensured to be below the dielectric strength of SiN_x. Meanwhile, a reversible leakage current is observed. "Reversible" in this context refers to the fact that the membrane remains insulating when an electric field is reverted to a low value and that ionic current through a membrane is invariably absent. We use a feedback control mechanism to monitor the current in real-time. The applied potential is terminated quickly following the detection of a

sudden increase in current, which corresponds to a hard dielectric breakdown[19] event and the creation of a nanopore.

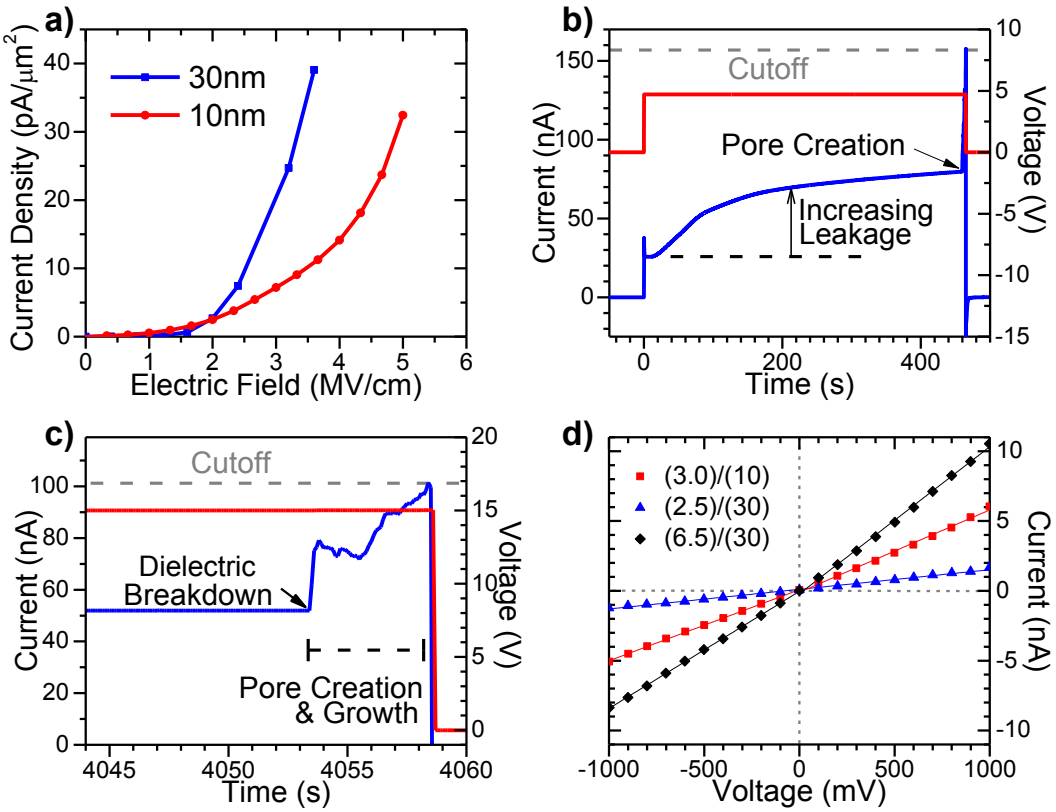

Figure 4.2: Current responses of membranes at different stage. a) Leakage current density of pristine 10nm and 30nm thick SiN_x membranes (without pore) under different electric field. b) Leakage current of a 10nm SiN_x membrane subjected to constant voltage bias of 5V. Leakage current for this experiment increased over time, thought to be due to trap-assisted tunneling. A rapid increase in current is observed at the end of the duration, at which a pore is created. The resulting pore is 5nm (18 nS) in diameter. c) Fine detail of the current response during a dielectric breakdown event on a 30-nm-thick SiN_x membrane, in 1M KCl pH10. Voltage bias is terminated upon reaching a pre-determined threshold current level, during which a pore is created and is allowed to grow. The resulting pore is 3-nm (2.9 nS) in diameter. d) Current-to-voltage curves for 3 nanopores fabricated on different membranes. The legend indicates the (pore diameter)/(membrane thickness) in nm. Measurements performed in 1 M KCl pH8, with an Axopatch 200B.

As shown in Figure 4.2b, leakage current changes slowly while the membrane is subjected to a constant voltage bias. This indicates that dielectric property of the thin film is being altered. Equivalently speaking, we can conclude that electronic structure of the SiN_x membrane is being changed under the electric stress. This is typical of time-dependent-dielectric breakdown (TDDB)[15,16,20,21]. The percolation theory developed by Degraeve *et al*. [22] is a comprehensive model to describe such phenomenon. We inflict this picture to relate how a nanopore is formed with a dielectric breakdown event. In the model, tunneling current is introduced to the membrane when it is subjected to an external electric field. The current can either be from Fowler–Nordheim tunneling or hot carrier injection [22]. In any case, electron traps are being randomly generated and accumulated in the bulk of the dielectric, as illustrated in Figure 4.3b. These electron traps, modeled as some spheres with a uniform radius, are more conductive than the bulk. Their presence allows electrons to hop from one trap to another easily, which can (but not necessarily) contribute to an increase in the observed tunneling current by trap-assisted mechanism[23–25]. This trap-assisted tunneling current can in turn generate more traps along its path[21,23–25], reinforcing a positive feed-back self-localization mechanism. When a critical electron trap density (CETD) is reached [22,26], overlapping traps form a conductive path between anode and cathode, as shown in Figure 4.3c, upon which a hard dielectric breakdown event occurs. This percolation model has several significant aspects relevant to nanopore fabrication. Firstly, each hard dielectric breakdown event corresponds to an individual localized conductive pathway, attributed to a single nanopore per dielectric breakdown event. Secondly, the model implies a stochastic nature to the occurrence of a dielectric breakdown event, described by Weibull distribution function[15,18,22]. As such, more than one dielectric breakdown event occurring simultaneously within the time resolution of our experimental setup is highly unlikely. This further reassures the fabrication of a unique nanopore at

each detected dielectric breakdown event. Lastly, the model predicted that the CETD is lowered for thinner membrane as it required fewer traps to span the thickness of the membrane. Likewise, the time variance for a dielectric breakdown is increased for the same reason. These are consistent with our observation on the time required to fabricate a nanopore.

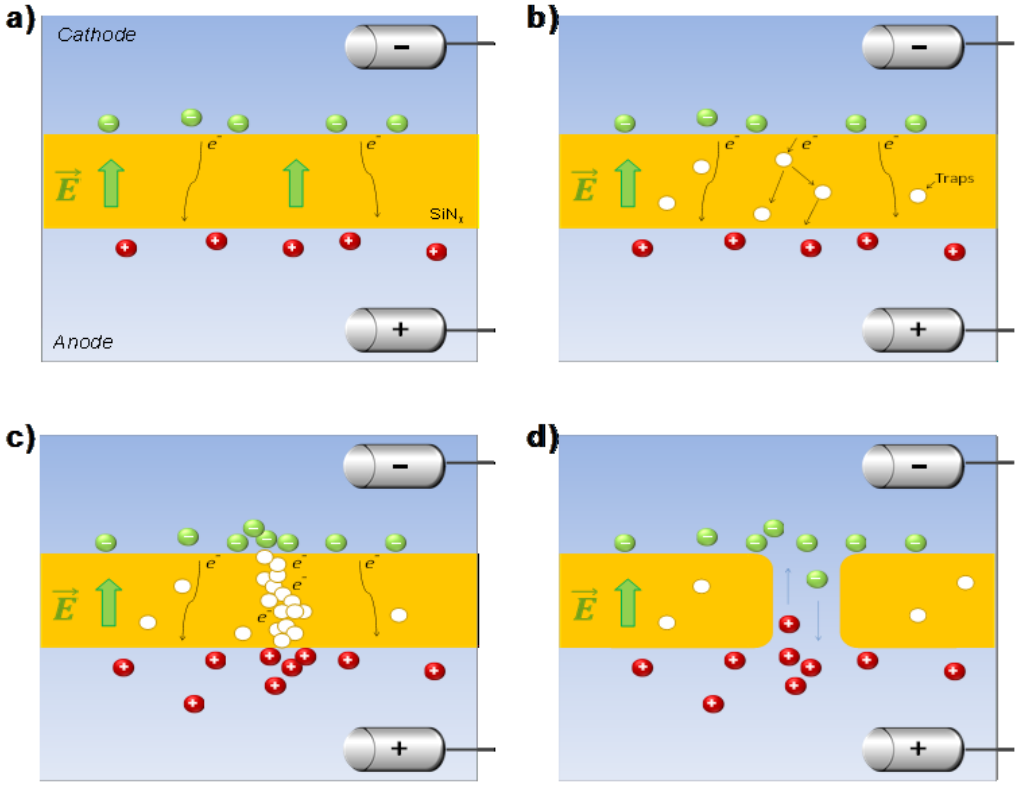

Figure 4.3: Illustration of a dielectric breakdown event. When a dielectric membrane is being stressed by an external electric field, stress induced leakage current (SILC) is observed. b) Stress from the field generated charge traps in the membrane. These traps facilitated additional tunneling current by trap-assisted tunneling (TAT) mechanism. Localized tunneling current can increase trap generation along its path. c) Percolation of charge traps, forming a localized conductive path between anode and cathode, at which a discrete dielectric breakdown event occur. d) A nanopore is formed when excess current during the dielectric breakdown removed material along the path.

Dielectric breakdown event in our system is unique. It is differentiated from the system assumed in most of the dielectric breakdown model, for the fact that our membrane is submerged in liquid. The presence of two electrolyte-dielectric interfaces complicated the scenario. In an electrolyte, ions are the charge carriers while in a dielectric material, electrons and holes carry the charge. For this reason, charge exchange must take place at the two interfaces when there is a tunneling current across the membrane. Different species of cations (K^+, Na^+, Li^+) are experimented and no differences were found in the dielectric breakdown behavior; results are shown in Figure 4.4c. Consider that these cations do not form stable redox product in water, then hydrogen, hydroxyl ions and possibly chlorine ions are likely involved in the charge exchange redox reactions. The products would be H_2, O_2 and Cl_2 gas dissolved in the electrolyte. In addition, hydrogen ions present at the inner Helmholtz layer can drift into the dielectric membrane driven by the electric field. This can cause physical damage to the silicon nitride[16,17,27]. To illustrate the involvement of hydrogen and hydroxyl ions, our fabrication method is tested with various 1M KCl electrolyte buffered at different pHs. As shown in Figure 4.4b, it is found that both high and low pH significantly shorten the time to a dielectric breakdown. The time of fabrication is reduced up to three orders of magnitude. In addition, as shown in Figure 4.4a, increasing voltage bias can also lead to an exponential decrease in fabrication time, which is intuitively expected. At pH 2 and 16V, a nanopore can be created on a 30nm membrane in seconds. When taking into account the simplified handling procedure, the effort and time required to fabricate a nanopore with this method is unmatched by all other current nanopore fabrication techniques. For this reason, this new method can potentially increase the scientific research throughput in the field in a substantial manner.

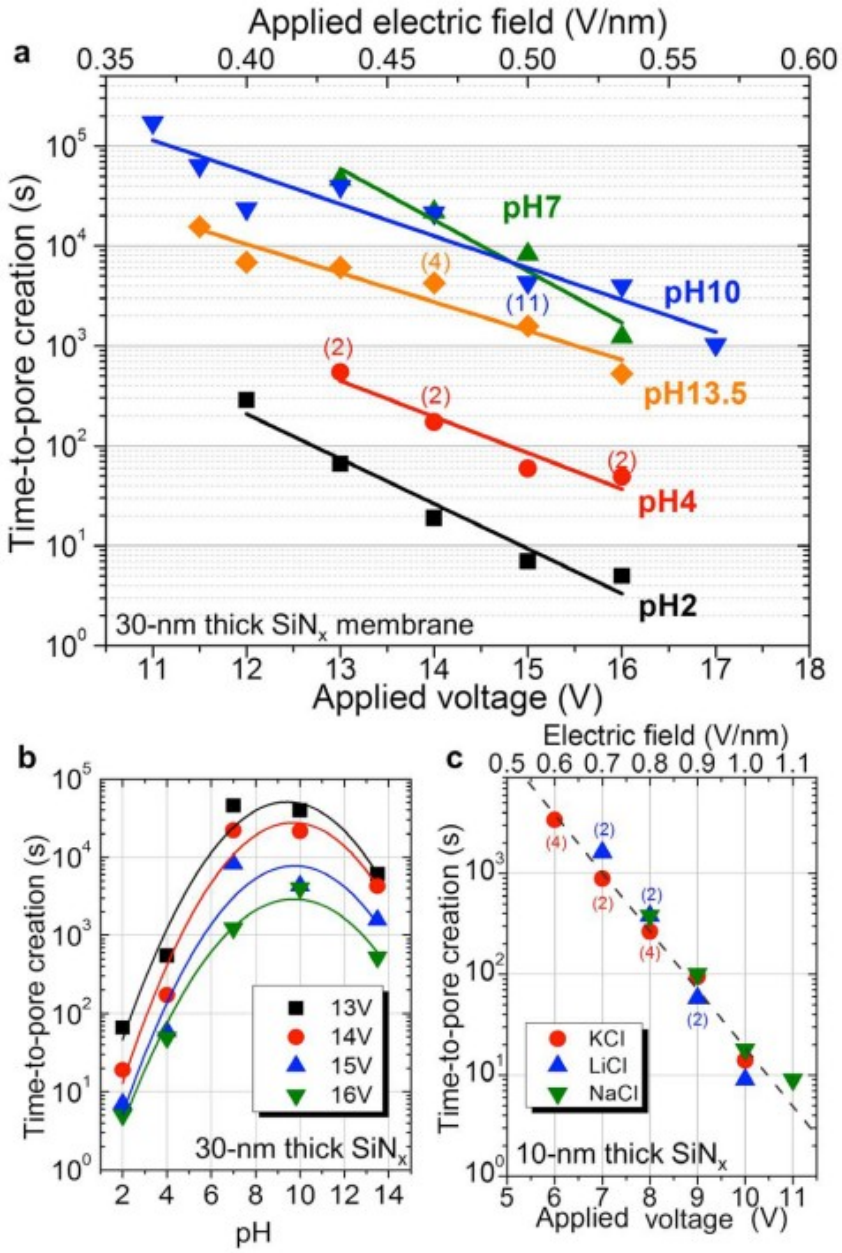

Figure 4.4: Time-to-pore creation as a function of experimental conditions. a) Semi-log plot of fabrication time of individual nanopores created in 30-nm-thick SiN_x membranes in 1M KCl buffered as indicated, versus the applied voltage and the calculated applied electric field. The number of separate nanopores each data point is averaged over is indicated in parentheses. The vast majority of nanopores plotted are sub-5-nm in size (i.e. ,7 nS). b) Semi-log plot of fabrication time versus pH for the data plotted in a). c) Semi-log plot of fabrication time of individual nanopores created in 10-nm-thick SiN_x membranes in 1 M Cl-based electrolyte buffered at pH 10 for different cationic species versus the applied voltage and the calculated applied electric field. All 66 nanopores plotted are sub-5-nm in size (i.e. ,20 nS).

4.2.2 Nanopore creation mechanism and control

The beginning of a hard dielectric breakdown event corresponds to the onset of the creation of a nanopore, during which a significant amount of current channels across the membrane through a localized conductive path. Consider tens of nano-amperes of current constricted in a nanometer square cross-section area would correspond to a current density beyond $10^7 A/cm^2$, which is the condition for electromigration of most metallic materials. Direct momentum transfer between electrons and atoms can knock atoms off the membrane directly into the electrolyte, ionizes the atoms to be dissolved or causes excess joule heating (thermal runaway). Electrochemical reaction can also facilitate dissolution or removal of atoms. Furthermore, electron traps are more energetic than atom in the bulk, which would have a lowered binding energy. The presence of electron traps on the conductive path would facilitate atoms removal. In any case, atoms are removed and a small nanopore is formed on the membrane. Currently, this process is controlled by a simple threshold feedback mechanism. Figure 4.2c shows a current trace during a dielectric breakdown event. A current threshold value about 200% of the baseline tunneling current is set as a cut-off condition. Upon the current reaching this value, the voltage bias is terminated. The system can take up to a few seconds trailing the onset of a dielectric breakdown before this threshold is reached. This simple threshold cut-off mechanism is found to be sufficient to produce small nanopore less than 4nm. Refers to Figure 4.2c, the current during the creation process can fluctuate rapidly. This is attributed to a violent modification of the material and also to the dissociation of water molecule when an ionic channel is formed. Because of the presence of this fluctuation, current level does not correlate strongly with the resulting pore diameter. Therefore, tightening the threshold value does not necessarily create a smaller pore. In some occasions, rapid termination of bias voltage can result in the absence of a pore altogether. In general, the resulting pore diameter is roughly

correlated with the cut-off time with respect to the onset of the dielectric breakdown. A future research approach might be to consider monitoring the energetic aspect of the current.

The phenomenon of dielectric breakdown is universal to all dielectric material. It is therefore reasonable to expect this new nanopore fabrication method to be applicable to different kinds of membranes. To validate this idea, we tested the method on thin membranes that are made of SiN_x, SiO_2, HfO_2 and Poly-methyl-methacrylate (PMMA). We confirmed that a nanopore can be fabricated on these membranes, which demonstrate the versatility of the method.

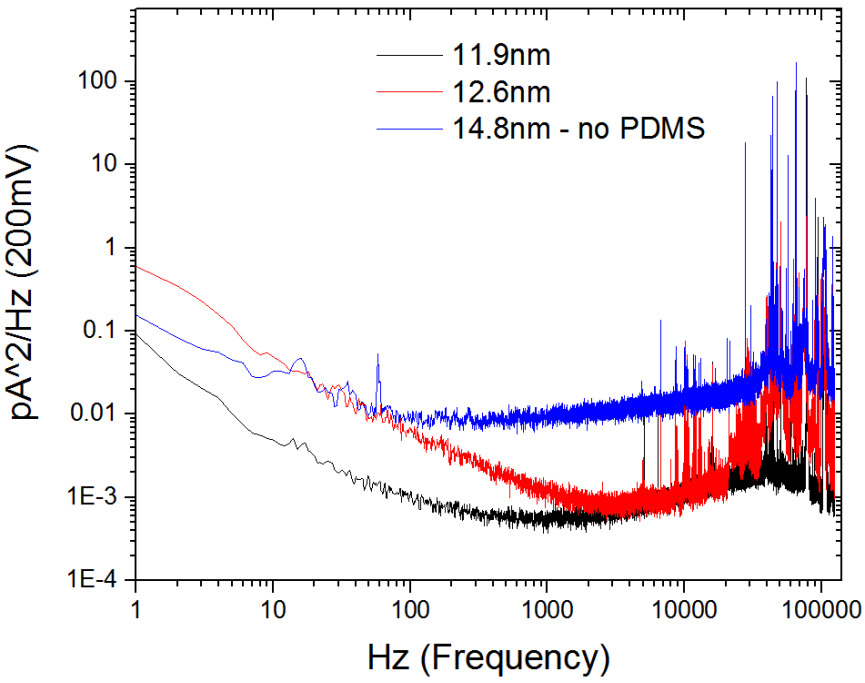

Figure 4.5: Power spectrum densities (PSD) of three nanopores fabricated by dielectric breakdown, taken at 200mV. The pore diameters are listed in the legend. They have a membrane thickness of 30nm. Exposed membrane area of two nanopore chips are covered by PDMS. The level of 1/f noise of nanopore created by dielectric breakdown are similar and sometimes slightly better than TEM drilled nanopore.

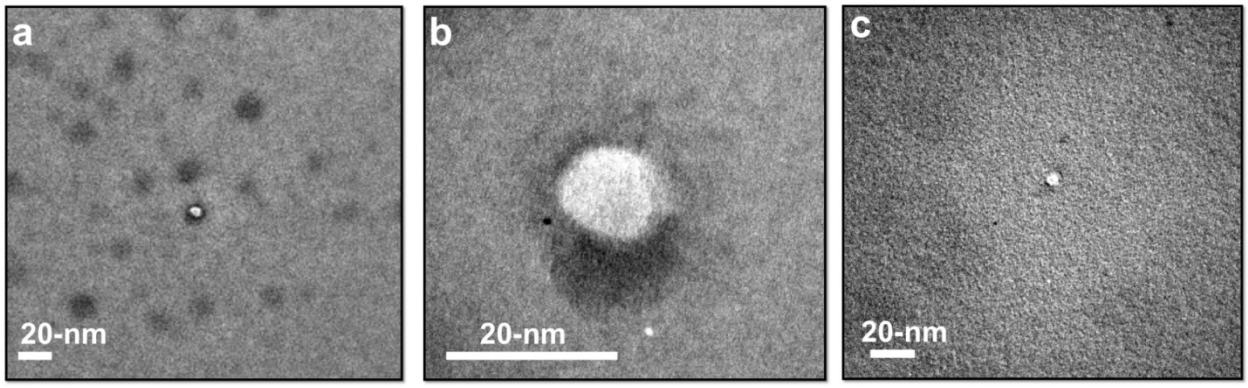

Figure 4.6: Bright Field TEM image of nanopores at different magnification. The pores sit on a custom 30nm thick SiN_x membrane, and are fabricated by dielectric breakdown. Dark spots appear on a) and b) are silicon-rich regions. a-b) a 14nm pore imaged at different magnifications. c) a 5nm pore. TEM image illustrated that pores fabricated by dielectric breakdown are circular in shape and have the two opening aligned.

4.2.3 Physical and Electrical Characterization

Physical dimension of a nanopore can be evaluated by its conductance, G, and can be related to an effective diameter, d, with[28,29]:

$$G = \sigma \left[\frac{4l}{\pi d^2} + \frac{1}{d}\right]^{-1} \quad (1)$$

where σ is the bulk conductivity of the solution and l is the length of a nanopore. Unlike pore drilled with TEM, we do not expect double cone geometry introduced by a converging electron beam. For this reason, effective length of a pore is taken as equal to thickness of the membrane. I-V characteristic are measured within ±1V range, where the leakage current is negligible. As shown in Figure 4.2d, nanopores we fabricated reveal an ohmic electric response in 1M KCl solution. Such I-V characteristics imply a relatively symmetric internal electric potential pore profile[30], which supports the symmetrical geometry with a uniform surface charge distribution assumed by our pore conductance model. To further characterize the nanopores, we examined the noise in the ionic

current with Fourier analysis. Figure 4.5 shows a series of power density spectrum (PSD) transform from some 200s of current traces on different pores. In order to have a meaningful measurement, noise from parasitic capacitance is minimized by first hand-painting a membrane with polydimethylsiloxane (PDMS) before a pore is being fabricated. The PDMS leaves only a small region on the membrane exposed to the electrolyte, which significantly reduce capacitive noise. As shown in Figure 4.5, our fabrication method consistently produces nanopores with low-1/*f* noise levels, compare favorably with TEM-drilled nanopores. Lastly, two nanopores 14nm and 5nm in diameter are imaged under a TEM, illustrated in Figure 4.6. The images show that the pores are circular in shape and have the two openings aligned on the same axis. Common intuition of dielectric breakdown from phenomenon like lighting tells us that a conduction path in a dielectric breakdown can sometimes be crooked or branched. The fact that the two openings are aligned illustrated that the initial conductive path takes the shortest direct route across the membrane, constricted by the thin membrane thickness. Examination of the pores under TEM, with tilting and contrast enhancing techniques, indicates that the rims of the pores are not thickened. This is a strong indication that the pores are created by removal of atoms instead of material reflow or shear rupturing, as one would expect material from the pore be conserved at its vicinity in those cases.

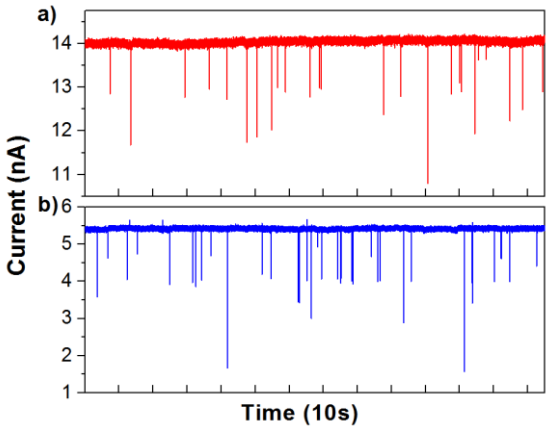

Figure 4.7: Current traces of electrophoretic DNA (10kbp) translocation experiment on different membrane materials. They illustrated that the method can create functional nanopore on different material. a) 7.2nm pore on 30nm SiN_x membrane, driven at 300mV. b) 6.5nm pore on a 20nm SiO_2 membrane, driven at 400mV.

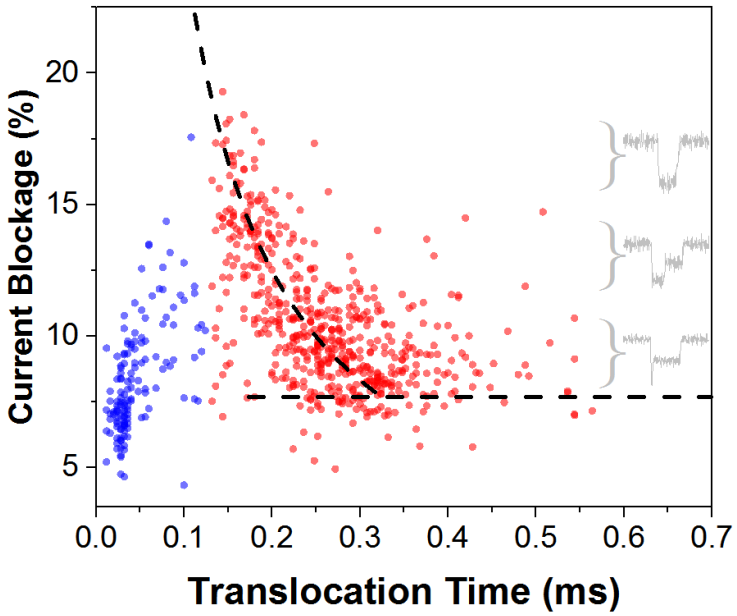

Figure 4.8: Scatter plot of individual DNA translocation event. Collusion events are marked as blue. These are events at which molecules partially entered the pore and then exited on the same side. Translocation events are marked as red. The horizontal dash line marks the single blockage level while the curve dash line marks ecd curve. Y-axis is the average blockage depth of an event normalized by the open pore current. Different blockage level corresponds to different folding configurations as a DNA molecule translocate.

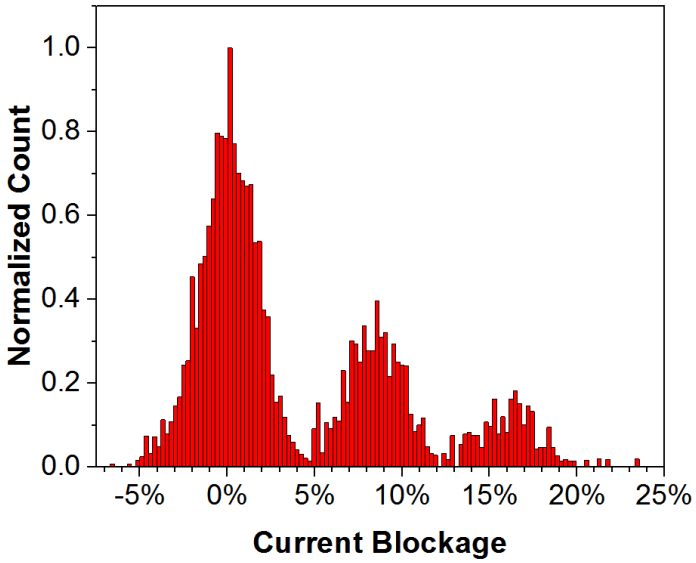

Figure 4.9: Accumulated histogram of current levels of 40 individual translocation events. Discrete peaks correspond to open pore, unfolded and single-folded DNA blockage level from left to right respectively.

4.2.4 Electrophoretic translocation of DNA molecules

To demonstrate that the method can create a nanopore on different materials, and to verify that these pores are equally functional compare to TEM-drilled nanopores, electrophoretic translocation experiments are performed with pores made of SiN_x and SiO_2. Figure 4.7 shows a section of two current traces. They correspond to the SiN_x and SiO_2 pore respectively. Each discrete drop in a current trace is referred to as a resistive-pulse. They are caused by the blocking of the pore during the translocation of individual lambda-phage DNA molecule (48.5 kbp, New England BioLabs). The appearance of discrete resistive-pulses clearly exemplifies that pores created by the method is functionally proficient for single-molecule sensing applications. However, our method of pore fabrication has a possibility of creating excessive dangling bonds on a pore wall, which can interact with analytes undesirably. To illuminate such concern, detail kinetics of the electrophoretic

translocations must be examined closely. Each individual resistive-pulse in the complete current trace from the SiN_x pore is extracted. The average blockage level of each individual pulse is plotted against the translocation time as a scatter plot shown in Figure 4.8. The figure illustrated that translocation events follow the trend of event charge deficit (ecd) curve[31], which is plotted as a curved dash-line. The ecd curve originates from the simple fact that a DNA molecule would take less time to translocate through a pore when it is folded, while at the same time have a higher blockage level in a proportional manner. This only holds when interaction between DNA molecules and pore wall is insignificant, as in the case of our pore. Lastly, instantaneous current from 40 individual translocation events are binned into an accumulative histogram as shown in Figure 4.9. Discrete peaks shown in the histogram correspond to different folded configurations of DNA molecules. The appearance of these peaks further illustrates the fact that these DNA molecules are undisturbed by the nanopore wall as they translocate.

4.3 Conclusion

This study illustrates a new nanopore fabrication method relying on dielectric breakdown. A quick charge of a membrane with a voltage bias can lead to the fabrication of a small nanopore. Experiments presented here show that nanopores fabricated by the new method are equally capable for single molecule sensing applications compare to TEM-drilled pores. Consider the tremendous reduction in complexity and cost over current techniques, we anticipate the new nanopore fabrication method can facilitate researches and applications in the related field.

4.4 Materials and Methods

4.4.1 Dielectric Membranes

Silicon Nitride (SiN_x) membranes used in our experiments are commercially available as transmission electron microscope (TEM) windows (Norcada product # NT005X and NT005Z). Each membrane is made of 10-nm or 30-nm thick low-stress (,250 MPa) SiNx, deposited on 200-µm thick lightly doped silicon (Si) substrate by low-pressure chemical vapour deposition(LPCVD). A 50-µm square window on the backside of the Si substrate is opened by a KOH anisotropic chemical etch. Prior to mounting into liquids, SiN_x membranes can be cleaned in oxygen plasma for 30 s at 30 W to facilitate wetting of the membrane surface, though this is not a requirement. All solutions used were filtered and degassed prior to use. The absence of pre-existing structural damages (e.g. pinholes, nano-cracks) is inferred by the fact that no current (,pA) is measured across a membrane at low voltages (< ±1 V) prior to nanopore fabrication. The membrane side opposing the Si etch pit is the reference point for all applied voltages in this article. Silicon dioxide membranes were also purchased from TEMWindows (product# SO100-A20Q33). Note that we have also successfully fabricated nanopores on SiN_x membranes purchased from TEMWindows, and on custom fabricated SiN_x membranes.

4.4.2 Instrumentation and Data Acquisition

A schematic of the experimental setup is shown in Figure 4.1a. A silicon chip with an intact silicon nitride membrane is sandwiched between two silicone gaskets (shown in purple on the figure). It is then positioned between the two electrolyte reservoirs in a PTFE (polytetrafluoroethylene) or a PEEK (polyether ether ketone) fluidic cell. The two reservoirs filled with liquid electrolyte are electrically connected to a current amplifier by two Ag/AgCl electrodes. The entire system is

encapsulated in a grounded faraday cage to isolate from electromagnetic interference. Data acquisition and measurement automation were performed using custom-designed LabVIEW software controlling a National Instruments USB-6351 or PXIe-6366 DAQ card. The value of the trans-membrane potential is set by the DAQ card. Leakage current is digitized at 250 kHz and the signal is filtered at 10 Hz. When a current exceed a pre-set threshold, the voltage bias is immediately ceased by the software (response time is ~100 ms). I-V measurements and ionic current signal during DNA translocations are recorded using an Axopatch 200B with a 4-pole Bessel filter set at 100 kHz, with at 250 kHz sampling rate. Data analysis was carried out using custom-designed LabVIEW software to measure the duration and depth of each current blockade events.

4.4.3 DNA Studies

We performed DNA translocation studies, using dsDNA fragments of 100 bp, 5 kbp, 10 kbp purchased from Fermantas (NoLimits products) in 1 M KCl pH8 or in 3.6 M LiCl pH8 at a final concentration of 10mg/mL. Lambda DNA (48.5 kbp) purchased from NewEngland BioLabs was also used.

References

(1) Li, J.; Stein, D.; McMullan, C.; Branton, D.; Aziz, M. J.; Golovchenko, J. a. Ion-Beam Sculpting at Nanometre Length Scales. *Nature* **2001**, *412*, 166–169.

(2) Klingfus, J.; Nadzeyka, A.; Bauerdick, S.; Albrecht, T.; Edel, J. B.; Gmbh, R. Wafer-Scale Ion Beam Lithography of Nanopore Devices. *Microsc. Microanal.* **2013**, *19*, 912–913.

(3) Cai, Q.; Ledden, B.; Krueger, E.; Golovchenko, J. a; Li, J. Nanopore Sculpting with Noble Gas Ions. *J. Appl. Phys.* **2006**, *100*, 24914–249146.

(4) Robert Louis Fleischer, Paul Buford Price, R. M. W. *Nuclear Tracks in Solids: Principles and Applications*; University of California Press, 1975; p. 569.

(5) Storm, a J.; Chen, J. H.; Ling, X. S.; Zandbergen, H. W.; Dekker, C. Fabrication of Solid-State Nanopores with Single-Nanometre Precision. *Nat. Mater.* **2003**, *2*, 537–540.

(6) Yusko, E. C.; Johnson, J. M.; Majd, S.; Prangkio, P.; Rollings, R. C.; Li, J.; Yang, J.; Mayer, M. Controlling Protein Translocation through Nanopores with Bio-Inspired Fluid Walls. *Nat. Nanotechnol.* **2011**, *6*, 253–260.

(7) Merchant, C. a; Healy, K.; Wanunu, M.; Ray, V.; Peterman, N.; Bartel, J.; Fischbein, M. D.; Venta, K.; Luo, Z.; Johnson, a T. C.; *et al.* DNA Translocation through Graphene Nanopores. *Nano Lett.* **2010**, *10*, 2915–2921.

(8) Renner, S.; Geltinger, S.; Simmel, F. C. Nanopore Translocation and Force Spectroscopy Experiments in Microemulsion Droplets. *Small* **2010**, *6*, 190–194.

(9) Luan, B.; Stolovitzky, G.; Martyna, G. Slowing and Controlling the Translocation of DNA in a Solid-State Nanopore. *Nanoscale* **2012**, *4*, 1068–1077.

(10) Meller, A.; Nivon, L.; Branton, D. Voltage-Driven DNA Translocations through a Nanopore. *Phys. Rev. Lett.* **2001**, *86*, 3435–3438.

(11) Skinner, G. M.; van den Hout, M.; Broekmans, O.; Dekker, C.; Dekker, N. H. Distinguishing Single- and Double-Stranded Nucleic Acid Molecules Using Solid-State Nanopores. *Nano Lett.* **2009**, *9*, 2953–2960.

(12) Division, B.; Biology, C.; Cruz, S. Characterization of Individual Polynucleotide Molecules Using a Membrane Channel. *Proc. Natl. Acad. Sci. U. S. A.* **1996**, *93*, 13770–13773.

(13) Venkatesan, B. M.; Bashir, R. Nanopore Sensors for Nucleic Acid Analysis. *Nat. Nanotechnol.* **2011**, *6*, 615–624.

(14) Rosenstein, J. K.; Wanunu, M.; Merchant, C. a; Drndic, M.; Shepard, K. L. Integrated Nanopore Sensing Platform with Sub-Microsecond Temporal Resolution. *Nature methods*, 2012, *9*, 487–492.

(15) Pey, K.; Wu, X.; Liu, W.; Li, X.; Raghavan, N.; Shubhakar, K.; Bosman, M. An Overview of Physical Analysis of Nanosize Conductive Path in Ultrathin SiON and High- Gate Dielectrics in Nanoelectronic Devices. In *Physical and Failure Analysis of Integrated Circuits (IPFA), 2010 17th IEEE International Symposium on the*; IEEE; pp. 1–12.

(16) Lombardo, S.; Stathis, J. H.; Linder, B. P.; Pey, K. L.; Palumbo, F.; Tung, C. H. Dielectric Breakdown Mechanisms in Gate Oxides. *J. Appl. Phys.* **2005**, *98*, 121301.

(17) Choudhury, A. I. K.; Mazumder, M. R. R.; Ahmed, K. Z.; Khosru, Q. D. M. EXPLANATION FOR REDUCED FOWLER-NORDHEIM TUNNELING CURRENT IN ULTRATHIN SILICON NITRIDE GATE DIELECTRIC. **2004**, 28–30.

(18) Sorsch, T. W.; Timp, G. L.; Baumann, F.; Liu, C. T.; Ma, Y.; Hwang, D.; Laboratories, B.; Technologies, L.; Ave, M.; Hill, M.; *et al.* Ultra-Thin Gate Dielectrics: They Break Down, But Do They Fail? **1997**, 73–76.

(19) Sune, J.; Nafria, M.; Aymerich, X. Reversible Dielectric Breakdown of Thin Gate Oxides in MOS Devices. *Microelectron. Reliab.* **1993**, *33*, 1031–1039.

(20) McPherson, J. W.; Mogul, H. C. Underlying Physics of the Thermochemical E Model in Describing Low-Field Time-Dependent Dielectric Breakdown in SiO2 Thin Films. *J. Appl. Phys.* **1998**, *84*, 1513.

(21) Schuegraf, K.; Hu, C. Hole Injection SiO2 Breakdown Model for Very Low Voltage Lifetime Extrapolation. *Electron Devices, IEEE Trans.* **1994**, *41*, 761–767.

(22) Degraeve, R.; Groeseneken, G. New Insights in the Relation between Electron Trap Generation and the Statistical Properties of Oxide Breakdown. *Electron Devices, ...* **1998**, *45*, 904–911.

(23) Wut, J.; Register, L. F.; Rosenbaumt, E. Trap- Assisted Tunneling Current Through Ultra-Thin Oxide. **1999**, 389–395.

(24) Nasyrov, K. a.; Shaimeev, S. S.; Gritsenko, V. a. Trap-Assisted Tunneling Hole Injection in SiO2: Experiment and Theory. *J. Exp. Theor. Phys.* **2009**, *109*, 786–793.

(25) Nasyrov, K. a.; Shaimeev, S. S.; Gritsenko, V. a. Trap-Assisted Tunneling Hole Injection in SiO2: Experiment and Theory. *J. Exp. Theor. Phys.* **2009**, *109*, 786–793.

(26) Entner, R. Modeling and Simulation of Negative Bias Temperature Instability.

(27) Oversluizen, G.; Zieren, V.; Johnson, M. T.; van der Put, a. a.; Lodders, W. H. M. Hot-Electron Degradation in Hydrogenated Amorphous-Silicon-Nitride Thin-Film Diodes. *J. Appl. Phys.* **2001**, *89*, 5491.

(28) Vodyanoy, I.; Bezrukov, S. M. Sizing of an Ion Pore by Access Resistance Measurements. *Biophys. J.* **1992**, *62*, 10–11.

(29) Kowalczyk, S. W.; Grosberg, A. Y.; Rabin, Y.; Dekker, C. Modeling the Conductance and DNA Blockade of Solid-State Nanopores. *Nanotechnology* **2011**, *22*, 315101.

(30) Kosińska, I. D. How the Asymmetry of Internal Potential Influences the Shape of I-V Characteristic of Nanochannels. *J. Chem. Phys.* **2006**, *124*, 244707.

(31) Fologea, D.; Gershow, M.; Ledden, B.; McNabb, D. S.; Golovchenko, J. a; Li, J. Detecting Single Stranded DNA with a Solid State Nanopore. *Nano Lett.* **2005**, *5*, 1905–1909.

Chapter 5

Long Passage Times of Short ssDNA Molecules through Metallized Nanopores Fabricated by Dielectric Breakdown

Published in Advanced Functional Materials
H. Kwok, M. Waugh, J. Bustamante, K. Briggs, and V. Tabard-Cossa, "Long Passage Times of Short ssDNA Molecules through Metallized Nanopores Fabricated by Controlled Breakdown," *Adv. Funct. Mater.*, vol. 24, no. 48, pp. 7745–7753, Oct. 2014.

Abstract

We describe the fabrication of individual nanopores in metallized dielectric membranes using controlled dielectric breakdown directly in solution. Nanopores, as small as 1.5-nm in diameter, are fabricated in Au-coated silicon nitride membranes immersed in 1M KCl by subjecting them to high electric fields. The physical and electrical characteristics of nanopores produced with this method are presented. We demonstrate the translocation of short single-stranded DNA molecules through such nanopore devices without further passivation of the metallic surface. We observe that metallized nanopores can prolong the translocation times of 50-nt ssDNA fragments by as much as two orders of magnitude, while the slowest events could reach an average speed as slow as 2 nucleotides per millisecond. The mechanism for the long dwell-time passage distribution is distinguished from prior studies, which relied on friction to slow down DNA, and is attributed to specific nucleotide-Au interactions.

5.1 Introduction

Solid-state nanopores are the subject of intense research efforts aimed at the development of disruptive, single-molecule sensing technologies with applications in DNA and protein sequencing.[1–3] Although electronic sequencing has been shown to be feasible using biological nanopores,[4–6] the robustness, flexibility in size and shape, and compatibility with wafer-scale technologies of solid-state nanopores still make them highly attractive, especially for the prospect of low-cost, scalable manufacturing of nanopore-based devices, and to diversify the breadth of applications. Yet, some challenges remain for solid-state nanopores to reach their full potential.

Sequence specific information obtained from ionic conductance measurements through a simple solid-state nanopore in an insulating membrane is generally limited.[7] The signal is bounded by physical constraints like instrumentation bandwidth, intrinsic electrical noise, spatial resolution, and thermal fluctuations.[8–10] For this reason, some groups have explored advanced functionalization of nanopore devices by designing more complex structures. These structures include multilayered membranes,[11,12] metallized dielectric membranes with or without molecular coatings,[13–15] and membranes equipped with nanoelectrodes.[16–20] In all these cases, the architecture of these advanced nanopore devices involve at least one conductive metallic film. Such conductive layers are intended to read alternative electrical signals, such as an induced charge,[21,22] potential[23] and transverse tunneling current,[24] or to control the motion of biopolymers during passage by modulating a local electric field[25], or by providing binding sites for biomolecules[14]. However, the throughput at which these complex structures can be tested under different operating conditions is a major bottleneck that impedes faster progress in the field. This is, in part, a consequence of the nanopore fabrication approaches currently being employed, which negatively affects the yield of

functional devices. Nanofabrication strategies relying on beams of energetic particles, either electrons or ions, require expensive, complex equipment that are inherently low throughput and involve multiple handling steps. Recently, our group has demonstrated that dielectric breakdown can be utilized to create individual nanopores on bare insulating solid-state membranes[26] and reliably achieve sub-2-nm feature size.[27] In addition, this technique creates nanopores directly in an aqueous solution, thus completely eliminating issues related to wetting and significantly reducing handling risks. The simplicity in fabrication and workflow offered by the method will likely help increase the research output of many groups and render the field accessible to others. Nevertheless, the capacity of this method to fabricate nanopores in more complex membrane structures remains to be explored. This article describes the fabrication of individual nanopores on metallized dielectric membranes using controlled dielectric breakdown, and introduces a high-electric field pulsing strategy where the voltage across the metallized membrane is stepped between a long, low monitoring-voltage and a short, higher fabrication-voltage. Finally, the translocation kinetics of short single-stranded DNA molecules through these metallized nanopores is presented. This study lays the foundation for future work to employ controlled dielectric breakdown for the fabrication of nanopores in more complex membrane structures, incorporating metallic materials, such as nanofluidic transistors or devices equipped with nanoelectrodes.

5.2 Results and Discussion

In previous work, we reported the fabrication of individual solid-state nanopores on bare SiN_x and SiO_2 membranes via controlled dielectric breakdown in solution.[26] The method allows for rapid and low-cost fabrication of nanopores for single-molecule detection simply by generating high

electric fields inside dielectric membranes using standard Ag/AgCl electrodes. This article extends a similar experimental protocol to fabricate individual nanopores on metallized dielectric membranes. In this work, we use 10-nm thick SiN_x membranes coated with 30-nm metal films (5-nm of Cr, 25-nm of Au) as described in the Methods section. To fabricate a nanopore, we mount the metallized membrane in a liquid cell so as to separate two reservoirs, which are filled with filtered and degassed 1M KCl, buffered at pH 10. To initiate the nanofabrication process, a leakage current across the metalized dielectric membrane is induced by applying a voltage across the two reservoirs in the range of 3-18 V. A custom resistive feedback current amplifier circuit connected to a computer is set to monitor the leakage current at 100-Hz. We have tested two different voltage schemes to expose the metallized membrane to high electric fields. The first approach follows reference 26, where a constant voltage is applied until a dielectric breakdown event occurs, at which point the leakage current abruptly increases and crosses a given threshold value, triggering the termination of the applied voltage. The second approach relies on the application a square voltage pulse between a low monitoring-voltage and a high fabrication-voltage. The monitoring voltage, set at 200 mV, is used to detect the presence of ionic current from a newly created nanopore. A current trace of each scheme is illustrated in Figure 5.1. In Figure 5.1b, the fabrication and monitoring pulse have a width of 50 ms and 1 S respectively. We found that both schemes can reliably fabricate a nanopore at either voltage polarity, and in conditions similar to fabrication on bare dielectric membranes. The pulsing approach eliminates the need to set an arbitrary leakage current threshold, which is experiment dependent, at the expense of a higher variance in fabrication time and overall longer fabrication process, since we anticipated that periods between fabrication pulses can possibly relax a predominate creation site or promote a new active site, thus resetting the

fabrication process (see supporting information section S1 for a list of tested fabrication conditions).

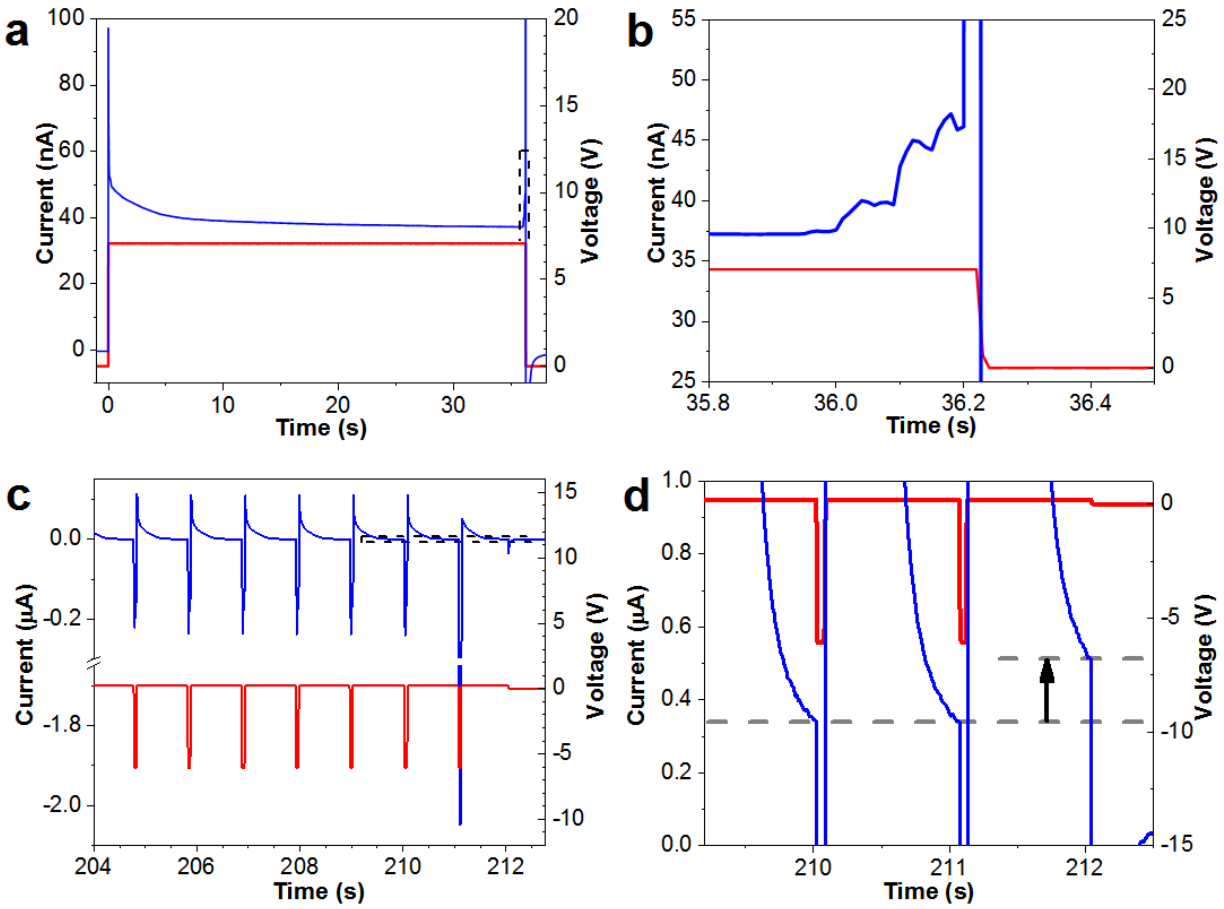

Figure 5.1: Current (Blue) and voltage (Red) trace during the fabrication of two metallized nanopores. They illustrated that dielectric breakdown can occur at both polarities and charging methods. The regions marked by a dash-rectangle in a) and c) are enlarged and illustrated in the figures b) and d) respectively. a) Creation with a constant applied voltage of +7 V. c) Creation with a repeating 50 ms pulse at -6 V. A monitoring period of 1 s, biased at 200 mV is inserted between each creation pulses. Spikes in both directions are caused by capacitive currents. d) The black arrow indicated the increase in current at the end of a monitoring period, attributed to the ionic conduction from a newly fabricated nanopore (created at around 211 s). The voltage bias is set to zero as ionic current is detected.

Physical conditions of nanopores and of the metallized membranes surfaces following fabrication by controlled dielectric breakdown were examined by optical microscopy and transmission electron microscopy (TEM). Optical examination of the metallized chip under a 63x stereomicroscope equipped with episcopic illumination revealed no observable physical changes to the Au film. The metallic layer remains intact and laminated. Under TEM, a 30-nm thick metalized layer is far less transmissive than bare SiN_x or vacuum, thus enabling high contrast imaging against a nanopore formed in the layered membrane, and somewhat facilitates the localization of a nanopore within the 50-μm × 50-μm membrane area. However, locating a sub-10-nm nanopore in a 2,500-μm^2 area remains challenging. Figure 5.2 shows two nanopores, created on two different Au-coated SiN_x membranes. The images show that a hole is formed through both the metal and the dielectric layer. From the TEM images, the opening through the Au layer appears to be larger than the hole in the silicon nitride, thus exposing some bare SiN_x around the rim of the nanopore. Furthermore, while the nanopore through the SiN_x layer has a cylindrical or elliptical shape, the opening through the metal layer appears to be conical, closing in size towards the nanopore. In figure 2a and 2b, the top opening on the metal surface is outlined by arrows. A schematic representation of the nanopore fabricated by controlled dielectric breakdown is shown in Figure 5.2c. The concentric and conical shape of the metallic opening may suggest that electrochemical etching, along the electric field lines extending away from the nanopore, is involved in the removal of Au and Cr as the nanopore was formed, in contrast to physical rupturing.

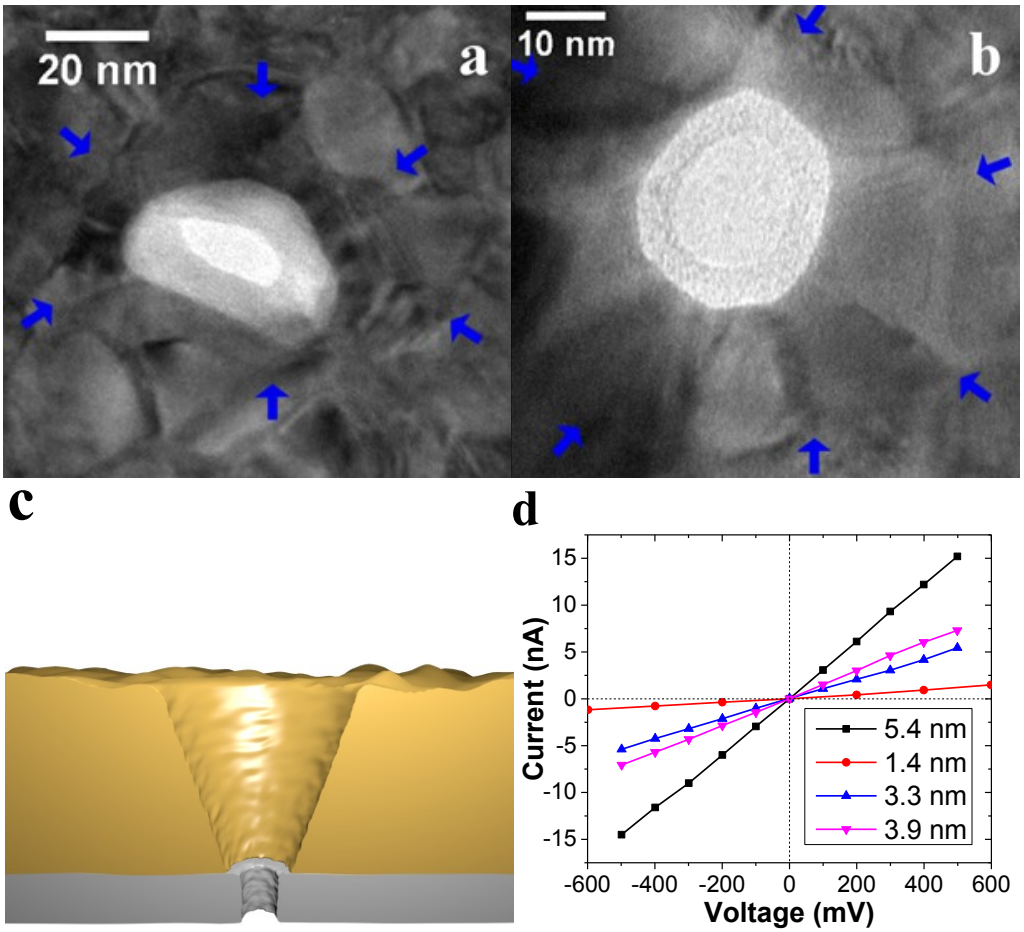

Figure 5.2: Bright field TEM images of two metallized nanopores, each with a different SiN_x membrane thickness, giving rise to a different contrast against a nanopore. Gold recedes away from, and is concentric to, the nanopore rim. Arrows outline the top opening of the metal channel. The effective diameter, *d*, and length, *l*, of the nanopores are : [a) *d* = 13-nm, *l* = 30-nm. b) *d* = 15-nm, *l* = 10-nm] c) Cross-section illustration of the geometry of a metallized nanopore, infered from TEM data. *d* = 5.4-nm *l* = 10-nm. d) I-V curves of 4 different metallized nanopores on 10-nm thick SiN_x membrane. Their diameters are listed in the legend.

Nanopores are electrically characterized immediately after fabrication by measuring their ionic current behaviour in 1M KCl pH10 and 3.6M LiCl pH8. Figure 5.2d shows I-V curves of 4 fabricated nanopores. On some occasions, we have observed the rapid enlargement of metallized nanopores at voltage bias greater than 500 mV. Although a nanopore can be enlarged by high

electric fields,[28] we have found that metallized nanopores are generally more susceptible to field-driven enlargement than bare silicon nitride nanopores. Considering that the metal is at equipotential with the electrolyte, the voltage drop is not only concentrated inside the nanopore in the SiN_x membrane but also at the Au/SiN_x interface, which we believe leads to enlargement under lower applied voltages. However, within a ±500 mV voltage range, these metallized nanopores exhibit ohmic I-V responses. The conductance extracted from these measurements can therefore be used to obtain physical dimensions for the nanopores. Assuming that the nanopore formed in the SiN_x layer has a cylindrical geometry, and that the metal layer is at equipotential with the electrolyte, then the length of a pore, l, is equal to the thickness of the SiN_x membrane and the thickness of the metal can be ignored. Hence the effective diameter, d, of a cylindrical nanopore is related to the conductance, G by:[14,29]

$$G(d) = \sigma \left[\frac{4l}{\pi d^2} + \frac{\alpha}{d}\right]^{-1} \tag{5.1}$$

In this equation, σ is the conductivity of the electrolyte inside the nanopore. The second term denotes the access resistance. When a pore is symmetrical with an access resistance on both side of pore opening, then $\alpha = 1$, while when access resistance on one side is suppressed by a metallic material, then $\alpha = 0.5$. Considering that ssDNA molecules can be captured from the metallized side, and that the applied voltage influences the capture rate, the electric field must also extend outside of the nanopore on the metallized side. Thus, α in the access resistance term can be taken to vary between 0.5 and 1. Diameters of nanopores calculated from conductance measurements using Equation 5.1 are compared with that obtained from DNA current blockages, and are presented in

Table 5.1. Results suggest that the cylindrical assumption with $\alpha \cong 0.5$ is reasonable and provides a good measurement of the nanopore effective size.

Table 5.1: Nanopore diameters calculated from open pore conductance (Eq. 5.1) and DNA blockage model (Eq. 5.2). Effective diameters are evaluated at both $\alpha = 0.5$ and $\alpha = 1$ as listed.

	Ionic Conductance Model (Eq1)			**DNA Blockage Model (Eq2)**	
V_{applied}	$I_{open\ pore}$	σ	$d\{\alpha = [0.5/1]\}$	$\Delta I/I$	$d\{\alpha = [0.5/1]\}$
-200 mV	6.1 ±0.5 nA	16.08 S/m	[5.4/6.0] ±0.2-nm	0.062 ±0.008	[5.4/5.2] ±0.3-nm
-300 mV	9.3 ±0.8 nA	16.08 S/m	[5.5/6.0] ±0.3-nm	0.062 ±0.015	[5.4/5.2] ±0.7-nm

We performed DNA translocation experiments to verify the ability of the metallized nanopores fabricated by high electric fields to detect individual DNA molecules and explored their translocation kinetics. Figure 5.3a showed a set of ionic current traces taken at -200 mV and -300 mV for a 5.4-nm nanopore, as calculated from conductance measurements in 3.6M LiCl (see Figure 5.2d) with $\alpha = 0.5$. Under this polarity, DNA molecules from the metal-coated side of the membrane are electrophoretically driven through the nanopore towards the SiN_x side of the membrane (see Methods). The ionic current blockages during the passage of 50-nt ssDNA are qualitatively similar to electrical signals observed on bare SiN_x membranes using either TEM-drilled nanopores or pores fabricated by controlled dielectric breakdown.[26] DNA capture rate is found to be dependent on applied voltage, corresponds to 1.5 Hz and 10.4 Hz for -200 mV and -300 mV respectively. Figure 5.3b, 3c and 3d show individual translocation events at -300 mV for linear, partially folded and fully folded ssDNA molecules accordingly.

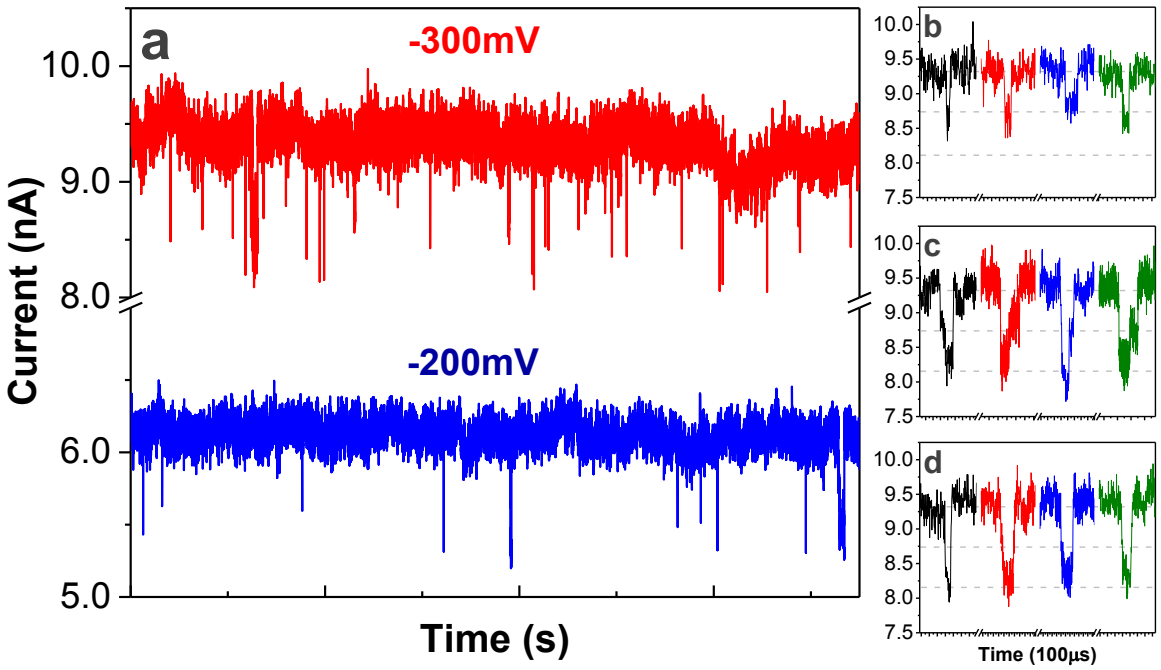

Figure 5.3: Ionic current traces of ssDNA translocations through the metallized pore a) driven at -200 mV and -300 mV. b-d) illustrations of some individual translocation events at -300 mV. The dashed line indicates the baseline current (9.32 nA), the expected single blockage level (6.25%) and the double blockage level (12.5%) calculated with Equation 2. Vertical axes are current in unit of nA. b) unfolded translocations, c) partially folded translocations, d) folded translocations.

Ionic blockage current level of single-level events, ΔI, caused by translocations of DNA molecules in a linear configuration provides an alternative method to estimate a pore size. Assuming a DNA molecule spans the entire length of a SiN_x pore when it translocates through, the normalized ionic blockage current is given by:[29]

$$\frac{\Delta I}{I} = \frac{\Delta G}{G(d)} = 1 - G(d')/G(d) \qquad (5.2)$$

where $d' = \sqrt{d^2 - d_{DNA}^2}$ is the effective cross-section diameter of a pore when a DNA molecule is present. A 50-nt ssDNA molecule, at the salt concentration we used, has a persistence length of around 2.2-nm[30] and a contour length of 33.8-nm. Since the contour length is longer than several persistence lengths, a molecule can translocate in a folded (two, or more, quantized current levels) or linear (unfolded, single-level events) conformation. The time-averaged ionic current blockage level of an event should then be bounded by the unfolded configuration and the highest-order possible folded configuration during passage. As shown in Figure 5.3, we predominately observe single and double blockage level, in agreement with the steric possibilities offered by the nanopore size. Substituting the experimental value of $\Delta I/I = 0.062$, for the average relative blockage level of linear conformation, into Equation 2 provides an alternative method to evaluate the effective pore diameter. Values are shown in Table 1. Using d_{DNA} = 1.4-nm yields an effective pore diameter of 5.4-nm, which agrees very well with the diameter acquired from conductance measurement with Equation 1, and supports the cylindrical geometry assumption using the nominal SiN_x membrane thickness as the nanopore length.

Figure 5.4a shows a scatter plot of the percent current blockage as a function of passage time for all translocation events obtained at -200 mV. Single level events, characteristics of the passage of linearized molecules, exhibit an average current blockage of 6.2% relative to the open pore current. Notably, translocation times for the passage of short 50-nt ssDNA molecules span multiple orders of magnitude, ranging from a few microseconds to tens of milliseconds. This clearly indicates that the event charge deficit (ecd), *i.e.* the measured time integral of blocked ionic current, is not conserved, which is contrary to what is expected for electrophoretically driven passage in pores of this size.[31] This is further revealed when ecd is plotted as a function of translocation time as shown

in Figure 5.4b, showing a non-zero slope. The non-conserved ecd implies that the average translocation speed varies greatly amongst strands of identical length, and suggests the presence of strong DNA-nanopore wall interactions.

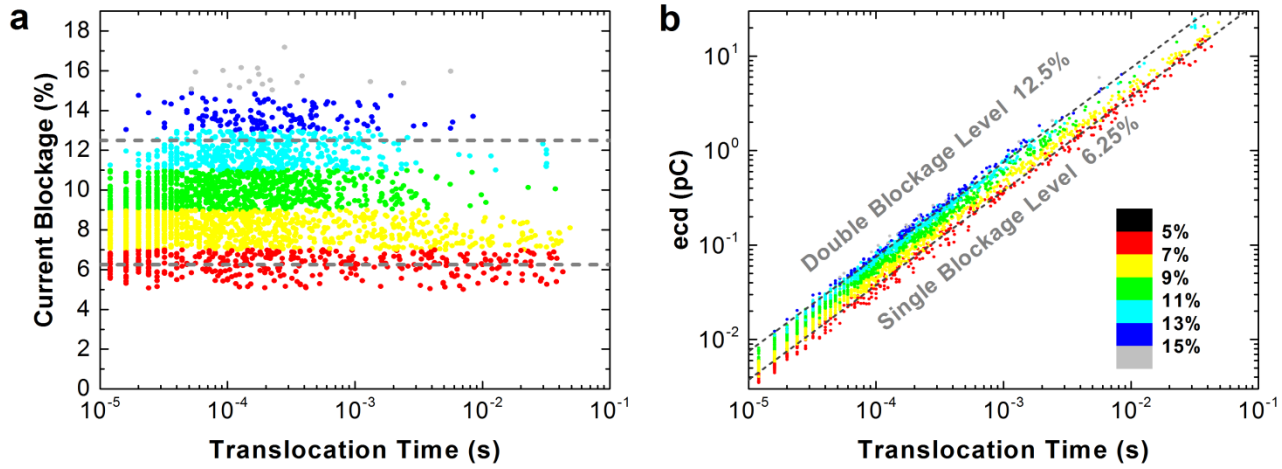

Figure 5.4: Data points are color-mapped to their relative current blockage level. The scale is shown on b). Data points on the left end are aligned vertically because of the limit of temporal resolution. a) Scatter plot of ssDNA translocation events at -200 mV. The relative blockage level is defined with respect to the open pore current. Translocation time is plotted in log scale. The two dashed lines represent the expected single and double blockage levels, 6.25% and 12.5% respectively, calculated with Equation 2. b) Log-log plot of ecd versus translocation time. The ecd of an event is the product of the translocation time and the time-averaged blockage current. Data points are color-mapped to their relative current blockage level.

Long dwell-time passage of short ssDNA shown in Figure 5.4a could potentially originate from two or more ssDNA fragments entering a pore simultaneously, though mutual repulsion should minimize such an occurrence. To verify that registered events are indeed full translocations of individual ssDNA molecules, ecd is plotted against the translocation time in log-log scale in Figure 5.4b. Multiple DNA molecules entering the pore simultaneously would cause higher current blockage levels than single-level events. If long lasting events were caused by multiple molecules

entering the pore simultaneously, the data points in Figure 5.4b would increasingly deviate away from the single blockage level as translocation time increases. On the contrary, the data points fall closely within the single and double blockage levels, and exhibit a straight line in log-log scale with a slope (power) of 1. Of note from Figure 5.4a and 4b is the fact that for very long translocation times (>3 ms) single-level events are favoured. This observation implies that the slowing down mechanism at play here is distinct from friction dominated kinetics previously observed on bare SiN_x pores, as one would expect folded ssDNA to cause increased friction with the nanopore wall.[32]

To highlight the slowed ssDNA translocation kinetics through metallized nanopores, we compare these results with data obtained on a bare SiN_x nanopore of similar size. Identical ssDNA translocation experiments were performed on the two separate nanopores at -200 mV. The observed ionic current blockade levels produced by the translocation of 50-nt ssDNA molecules on a bare SiN_x nanopore compare very well with the data on metallized nanopore (see Table 1). This further supports our assumption that most of the potential drop is across the insulating silicon nitride portion of the membrane for metallized nanopores fabricated by controlled dielectric breakdown. The two nanopores must therefore have similar effective diameters and lengths. The normalized histograms of log-translocation time are shown in semi-log scale in Figure 5.5. It is clear that metallized nanopores significantly extend the translocation time, by as much as two orders of magnitude, with the median prolonged by roughly one order of magnitude. The upper bound of translocation times corresponds to an average speed of 2 ms per nucleotide, although we do not expect nucleotides in a strand to necessarily translocate at a uniform speed. It is more likely that given the strong adenine-Au interactions,[33–35] a single-stranded polyadenine DNA molecule would

be temporarily interrupted by the Au surface as it translocate due to their binding affinity. Besides the extended translocation times, the distribution is also highly heavy-tailed, characterized by a non-linear decay when plotted in log scale, implying that the observed long lasting translocations events are not rare.

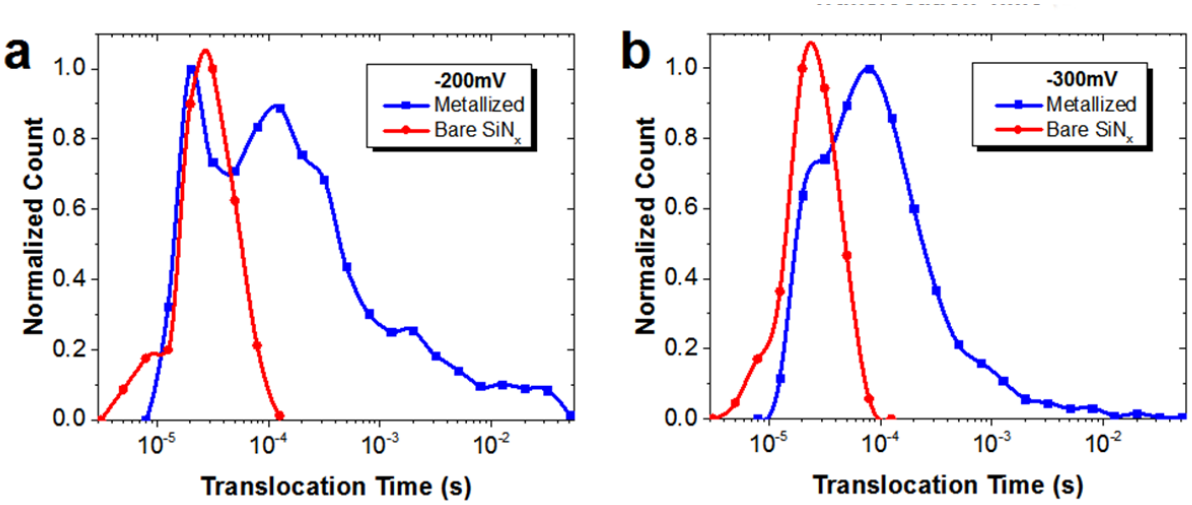

Figure 5.5: Histogram of log-translocation-time taken at -200mV and -300mV respectively to a) and b). Counts of each set are normalized to their maximum value for the purpose of comparison. Translocation experiments are carried out on a bare SiN_x nanopore (d = 5.2-nm, l = 10-nm) and the metallized nanopore (d = 5.4-nm, l = 10-nm). Solid spline lines are used to connect the data points within a set.

Further investigation of the histogram data between metallized and bare SiN_x nanopores indicates that there are two distinguishable peaks in a distribution for the metallized nanopore data. Considering the fact that the peaks at the lower bound from both sets of data overlap closely, we argue that this sub-population of translocation events originates from translocations in the absence of, or with very weak, Au-DNA interactions. Based on the metallic nanopore geometry extracted from TEM images (Figure 5.2), which indicates that the Au layer is slightly receded from the edge

of the nanopore formed in the SiN_x layer, it is possible for a DNA molecule to be captured by the pore and to translocate close to the central axis, without coming into contact with the metal surface.

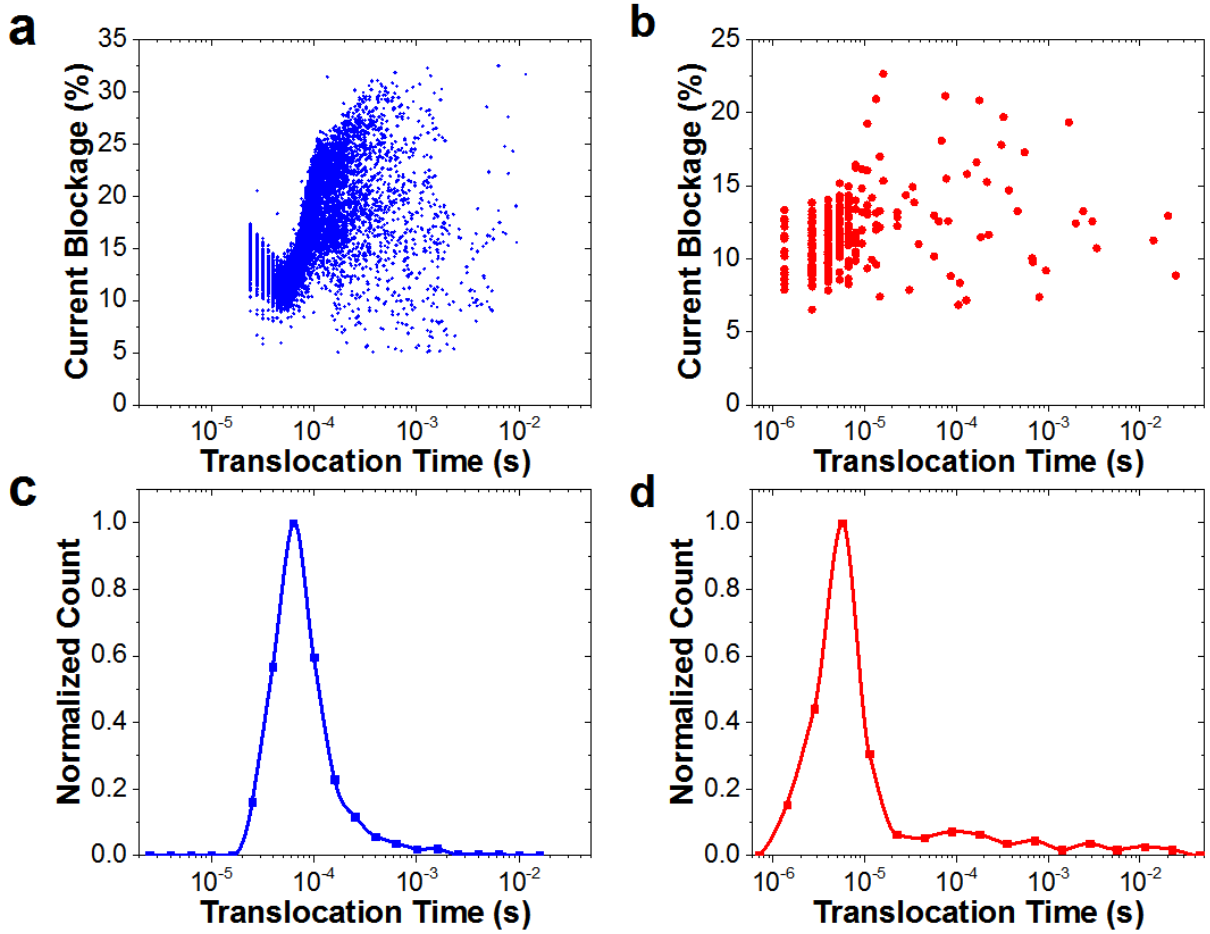

Figure 5.6: Scatter Plot of translocation events a) Scatter plot of 13577 translocation events. 50-nt ssDNA fragments are driven at +200mV, at which strands enter the metallized pore (d = 4.9-nm, l = 10-nm) from the silicon nitride side. b) Scatter plot of 398 events of 50-bp dsDNA fragments translocate through a metallized pore (d = 5.8-nm, l = 10-nm), from the metallic side, driven at -300mV. Data are sampling at 750kHz. Figure c) and d) are normalized histogram of translocation time of a) and b) respectively. A segment of the corresponding current traces are given in supporting information S4.

To identify the nature of the interaction, two additional experiments were performed. The first experiment involves translocating 50-nt ssDNA fragments in the reverse direction (from SiN_x to metallic side). In this direction, DNA strands will not encounter the metallic layer until they translocate through the nanopore. With this experiment, interaction of ssDNA with the silicon

nitride pore wall and the metallic layer can be distinguished. A metallized pore with d = 4.9-nm is utilized for the experiment. Scatter plot and histogram of the translocation time is shown in Figure 5.6a and 6c respectively. Refers to the scatter plot, current blockage appears to increases as a function of translocation time. This suggested that ssDNA have some frictional interaction with the silicon nitride pore wall. While ssDNA has the nucleotides hydrogen bonds exposed, some degree of interaction is not unexpected. However, in contrast to Figure 5.5, translocation in the reverse direction do not exhibit double peaks or significant broadening in the histogram as shown in Figure 5.6c. The mildly prolonged translocations are not reflected in the histogram. This indicates that the frictional interaction only affected a small population of the events, and is not applicable to explain the prolonged events seen in the forward translocation experiment. This leaves the gold-DNA interaction a likely explanation. Next is to answer the question whether the gold interacted with the backbone or the nucleotides of an ssDNA. To address the issue, a second experiment is performed, which involves driving 50bp double-stranded DNA (dsDNA) fragments to translocation through a metalized nanopore. Results are shown in Figure 5.6b and 5.6d. The histogram in 5.6d shows a distinct narrow peak, implying weak dsDNA – gold interaction.

Experimental data presented in this article point to the fact that the gold layer is interacting strongly with the ssDNA and is likely the cause of the exceptionally long translation times. This is consistent with prior knowledge that ssDNA can be physisorbed to gold surfaces in a base specific way.[33–35] In particular, adenine interacts with gold most strongly. Accordingly, we can present the following picture that would be in line with the observations. Figure 5.7 illustrates the two possible scenarios when a ssDNA molecule is electrophoretically driven from the metal side to SiN_x side. In Figure 5.7a, both ends of the ssDNA are physisorbed onto the gold surface leading to a folded entry

of the molecule into the SiN_x portion of the nanopore, thus producing long-lived double-level events. In Figure 5.7b, during capture most of the ssDNA fragment is physisorbed onto the gold surface, leaving only one short end of the ssDNA to enter the pore, leading to single-file passage. These single-level events can be longer-lived than folded translocations if they initially experience less electrophoretic pulling force due to a smaller number of nucleotides inside the pore, while also experiencing stronger pinning from the longer proportion of their chain being physisorbed to the gold. This would explain why prolonged data points are inclined toward the single blockage level.

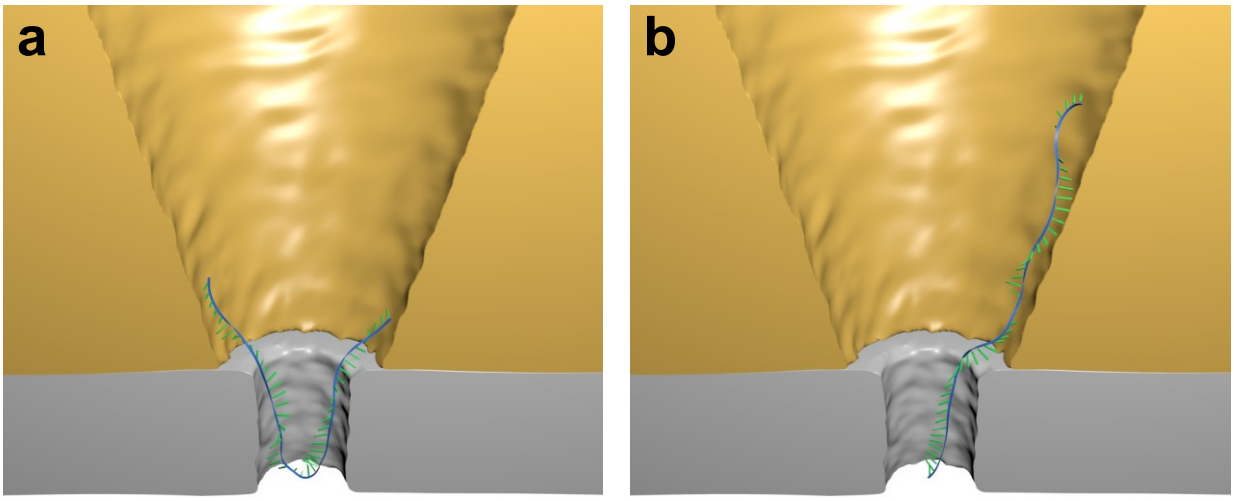

Figure 5.7: Illustration of translocation dynamics of a 50-nt ssDNA through a metallic nanopore. The ssDNA has a contour length of 33-nm. The SiN_x nanopore has dimensions: d = 6-nm, l = 10-nm. Arrows depict the direction of translocation. a) Small segments of ssDNA chain are being absorbed to the metallic surface at both ends of the molecule. b) A large segment of ssDNA chain is being absorbed to the metallic surface.

5.3 Conclusion

In summary, we demonstrated that controlled dielectric breakdown can be utilized to fabricate more complex nanopore structure comprising of both metallic and dielectric materials. We further

showed that metallized nanopores produced using such method are compatible with single molecule sensing of DNA molecules. The metal layer in the vicinity of the opening of the nanopore interacts strongly with polyadenine single-stranded DNA, resulting in exceptionally long passage times for these short molecules. The observed translocation kinetics is believed to be selective based on the initial molecular conformation and the length of DNA interacting with the metallic surface, since we anticipate this work will provide a new strategy to fabricate a nanopore equipped with nanoelectrodes for sequencing applications by single-molecule tunnelling spectroscopy.

5.4 Methods

5.4.1 Metal Deposition on Membrane

In this study, we employed commercially available free-standing silicon nitride membranes 50-μm×50-μm in size located at the center of a 3-mm in diameter, 200-μm thick silicon support chip, as the starting point of our fabrication process (TEM windows from Norcada NT005Z and NT005X). These TEM windows have a 10-nm or 30-nm thick non-stoichiometric silicon nitride (SiN_x) layer, deposited by low-pressure chemical vapor deposition (LPCVD). The resulting silicon nitride is amorphous, slightly silicon rich and low in tensile stress. Prior to metal deposition via e-beam evaporation, the SiN_x membranes are plasma cleaned at 30 W for 60 s. A 5-nm Cr adhesive layer is first deposited, followed by 25-nm of Au. The metallic layer is deposited onto a circular area of ca. 1-mm in diameter at the center of the chip, defined by an Al shadow mask. This prevents metals from being deposited on the edge of a chip, where the insulating SiN_x is often damaged, exposing the doped silicon substrate, which could create an alternative electrical pathway for the leakage current across the two sides of the chip.

5.4.2 Mounting and Wetting Procedures

The metallized membrane is placed in a custom designed polyether ether ketone (PEEK) cell as to separate two 200-μL fluidic reservoirs, each containing an Ag/AgCl electrode. Custom silicone elastomer gaskets are used to form a liquid tight seal between the two sides of the membrane. To ensure proper wetting of the membrane, each reservoir is first filled with 95% ethanol before switching to water and finally the aqueous salt solution used for fabrication. All solutions used were filtered and thoroughly degassed. Since the wet state of the membrane cannot be directly verified by resistance measurement, we instead evaluate the capacitance of the immersed chip with a digital multimeter (Agilent 34405A). For our experimental setup, when the membrane is fully wetted, a capacitance value >200 pF is measured in 1M KCl.

5.4.3 DNA Translocation Measurements and Analysis

For ssDNA translocation experiments, ionic current through a nanopore is monitored by a commercial patch-clamp amplifier (Axopatch 200B), with a 4-pole Bessel filter set at 100 kHz. Current traces are digitized at 250 kHz by a DAQ card (National Instruments, PXI-6361) and then recorded in a computer using custom LabView software. Short single-stranded DNA (ssDNA), 50-nt in length, with sequence $(dA_9dC)_5$, synthesized by Integrated DNA Technologies Inc, are used in this study. For dsDNA experiment, commercial patch-clamp amplifier (Multiclamp 700B) is used, with analog filter bypassed while sampling at 750kHz. Commercial DNA products, *NoLimits DNA fragments 50bp* from Thermal scientific are used for the experiments. All DNA translocations are performed in 3.6M LiCl, 10mM HEPES pH8. Li^+ is used to promote slower translocation times due to the stronger screening of the DNA charge compared to K^+.[36] In all experiments, 100-pmole of ssDNA was mixed thoroughly with 200-μL of electrolyte at the cathode reservoir, yielding a molar

concentration of 0.5-nM. Throughout this work, the reference point (ground) for all voltages quoted is the silicon nitride side of the membrane (*i.e.* opposite to the metallic side). Translocation events, registered as discrete drops in current, are detected and analyzed by custom LabView software. The relatively large area of metal exposed to the electrolyte gives rise to significant high-frequency noise, due to the increased chip capacitance compared to uncoated membranes.[8,13] If an experiment required, this extra noise could be removed by patterning of the metal layer[13] or by painting PDMS[8] to reduce the surface area of the metal exposed to the electrolyte. In addition, ssDNA strands can be physisorbed onto the Au surface near the nanopore entrance, which can cause low-frequency current fluctuations (see supplementary information section S2 for noise characterization of our devices). In our experimental configuration, a ~5.4-nm pore detecting ssDNA fragments has a signal-to-noise ratio of ~2. This ratio improves to 3 when the data is digitally low-pass filtered at 20 kHz. However, even at this ratio, errors can occur while evaluating the translocation time of an event. Due to the large number of events detected, the error rate is estimated by sampling a random subset of data points at different orders of magnitudes in translocation time (see supplementary information section S3).

Acknowledgments

This work was supported by the Natural Sciences and Engineering Research Council of Canada (NSERC), and the Canada Foundation for Innovation. J. Bustamante, K. Briggs and M. Waugh acknowledge the financial support provided by SENESCYT, NSERC, and OGS respectively, for Postgraduate Fellowships. The authors would like to thank Y. Liu for valuable technical support during TEM imaging.

References

(1) Nivala, J.; Marks, D. B.; Akeson, M. Unfoldase-Mediated Protein Translocation through an A-Hemolysin Nanopore. *Nat. Biotechnol.* **2013**, *31*, 247–250.

(2) Zhao, Y.; Ashcroft, B.; Zhang, P.; Liu, H.; Sen, S.; Song, W.; Im, J.; Gyarfas, B.; Manna, S.; Biswas, S.; *et al.* Single-Molecule Spectroscopy of Amino Acids and Peptides by Recognition Tunnelling. *Nat. Nanotechnol.* **2014**, *9*, 466–473.

(3) Branton, D.; Deamer, D. W.; Marziali, A.; Bayley, H.; Benner, S. a; Butler, T.; Di Ventra, M.; Garaj, S.; Hibbs, A.; Huang, X.; *et al.* The Potential and Challenges of Nanopore Sequencing. *Nat. Biotechnol.* **2008**, *26*, 1146–1153.

(4) Clarke, J.; Wu, H.-C.; Jayasinghe, L.; Patel, A.; Reid, S.; Bayley, H. Continuous Base Identification for Single-Molecule Nanopore DNA Sequencing. *Nat. Nanotechnol.* **2009**, *4*, 265–270.

(5) Cherf, G. M.; Lieberman, K. R.; Rashid, H.; Lam, C. E.; Karplus, K.; Akeson, M. Automated Forward and Reverse Ratcheting of DNA in a Nanopore at 5-Å Precision. *Nat. Biotechnol.* **2012**, *30*, 344–348.

(6) Manrao, E. a; Derrington, I. M.; Laszlo, A. H.; Langford, K. W.; Hopper, M. K.; Gillgren, N.; Pavlenok, M.; Niederweis, M.; Gundlach, J. H. Reading DNA at Single-Nucleotide Resolution with a Mutant MspA Nanopore and phi29 DNA Polymerase. *Nat. Biotechnol.* **2012**, *30*, 349–353.

(7) Venta, K.; Shemer, G.; Puster, M.; Rodríguez-Manzo, J. a; Balan, A.; Rosenstein, J. K.; Shepard, K.; Drndić, M. Differentiation of Short, Single-Stranded DNA Homopolymers in Solid-State Nanopores. *ACS Nano* **2013**, *7*, 4629–4636.

(8) Tabard-Cossa, V.; Trivedi, D.; Wiggin, M.; Jetha, N. N.; Marziali, A. Noise Analysis and Reduction in Solid-State Nanopores. *Nanotechnology* **2007**, *18*, 305505.

(9) Uram, J. D.; Ke, K.; Mayer, M. Noise and Bandwidth of Current Recordings from Submicrometer Pores and Nanopores. *ACS Nano* **2008**, *2*, 857–872.

(10) Zwolak, M.; Di Ventra, M. Colloquium: Physical Approaches to DNA Sequencing and Detection. *Rev. Mod. Phys.* **2008**, *80*, 141–165.

(11) Venkatesan, B. M.; Estrada, D.; Banerjee, S.; Jin, X.; Dorgan, V. E.; Bae, M.-H.; Aluru, N. R.; Pop, E.; Bashir, R. Stacked Graphene-Al2O3 Nanopore Sensors for Sensitive Detection of DNA and DNA-Protein Complexes. *ACS Nano* **2012**, *6*, 441–450.

(12) Harrer, S.; Waggoner, P. S.; Luan, B.; Afzali-Ardakani, A.; Goldfarb, D. L.; Peng, H.; Martyna, G.; Rossnagel, S. M.; Stolovitzky, G. A. Electrochemical Protection of Thin Film Electrodes in Solid State Nanopores. *Nanotechnology* **2011**, *22*, 275304.

(13) Wei, R.; Pedone, D.; Zürner, A.; Döblinger, M.; Rant, U. Fabrication of Metallized Nanopores in Silicon Nitride Membranes for Single-Molecule Sensing. *Small* **2010**, *6*, 1406–1414.

(14) Krishnakumar, P.; Gyarfas, B.; Song, W.; Sen, S.; Zhang, P.; Krstić, P.; Lindsay, S. Slowing DNA Translocation through a Nanopore Using a Functionalized Electrode. *ACS Nano* **2013**, *7*, 10319–10326.

(15) Wei, R.; Gatterdam, V.; Wieneke, R.; Tampé, R.; Rant, U. Stochastic Sensing of Proteins with Receptor-Modified Solid-State Nanopores. *Nat. Nanotechnol.* **2012**, *7*, 257–263.

(16) Sadki, E. S.; Garaj, S.; Vlassarev, D.; Golovchenko, J. a.; Branton, D. Embedding a Carbon Nanotube across the Diameter of a Solid State Nanopore. *J. Vac. Sci. Technol. B Microelectron. Nanom. Struct.* **2011**, *29*, 053001.

(17) Puster, M.; Rodríguez-Manzo, J. A.; Balan, A.; Drndić, M. Toward Sensitive Graphene Nanoribbon-Nanopore Devices by Preventing Electron Beam-Induced Damage. *ACS Nano* **2013**, *7*, 11283–11289.

(18) Healy, K.; Ray, V.; Willis, L. J.; Peterman, N.; Bartel, J.; Drndić, M. Fabrication and Characterization of Nanopores with Insulated Transverse Nanoelectrodes for DNA Sensing in Salt Solution. *Electrophoresis* **2012**, *33*, 3488–3496.

(19) Ivanov, A. P.; Instuli, E.; McGilvery, C. M.; Baldwin, G.; McComb, D. W.; Albrecht, T.; Edel, J. B. DNA Tunneling Detector Embedded in a Nanopore. *Nano Lett.* **2011**, *11*, 279–285.

(20) Ivanov, A. P.; Freedman, K. J.; Kim, M. J.; Albrecht, T.; Edel, J. B. High Precision Fabrication and Positioning of Nanoelectrodes in a Nanopore. *ACS Nano* **2014**, *8*, 1940–1948.

(21) Liu, Y.; Huber, D. E.; Tabard-Cossa, V.; Dutton, R. W. Descreening of Field Effect in Electrically Gated Nanopores. *Appl. Phys. Lett.* **2010**, *97*, 143109.

(22) Liu, Y.; Sauer, J.; Dutton, R. W. Effect of Electrodiffusion Current Flow on Electrostatic Screening in Aqueous Pores. *J. Appl. Phys.* **2008**, *103*, 084701.

(23) Sigalov, G.; Comer, J.; Timp, G.; Aksimentiev, A. Detection of DNA Sequences Using an Alternating Electric Field in a Nanopore Capacitor. *Nano Lett.* **2008**, *8*, 56–63.

(24) Lagerqvist, J.; Zwolak, M.; Di Ventra, M. Fast DNA Sequencing via Transverse Electronic Transport. *Nano Lett.* **2006**, *6*, 779–782.

(25) Luan, B.; Peng, H.; Polonsky, S.; Rossnagel, S.; Stolovitzky, G.; Martyna, G. Base-By-Base Ratcheting of Single Stranded DNA through a Solid-State Nanopore. *Phys. Rev. Lett.* **2010**, *104*, 238103.

(26) Kwok, H.; Briggs, K.; Tabard-Cossa, V. Nanopore Fabrication by Controlled Dielectric Breakdown. *PLoS One* **2014**, *9*, e92880.

(27) Briggs, K.; Kwok, H.; Tabard-Cossa, V. Automated Fabrication of 2-Nm Solid-State Nanopores for Nucleic Acid Analysis. *Small* **2014**, *10*, 2077–2086.

(28) Beamish, E.; Kwok, H.; Tabard-Cossa, V.; Godin, M. Precise Control of the Size and Noise of Solid-State Nanopores Using High Electric Fields. *Nanotechnology* **2012**, *23*, 405301.

(29) Kowalczyk, S. W.; Grosberg, A. Y.; Rabin, Y.; Dekker, C. Modeling the Conductance and DNA Blockade of Solid-State Nanopores. *Nanotechnology* **2011**, *22*, 315101.

(30) Chi, Q.; Wang, G.; Jiang, J. The Persistence Length and Length per Base of Single-Stranded DNA Obtained from Fluorescence Correlation Spectroscopy Measurements Using Mean Field Theory. *Phys. A Stat. Mech. its Appl.* **2013**, *392*, 1072–1079.

(31) Fologea, D.; Gershow, M.; Ledden, B.; McNabb, D. S.; Golovchenko, J. a; Li, J. Detecting Single Stranded DNA with a Solid State Nanopore. *Nano Lett.* **2005**, *5*, 1905–1909.

(32) Larkin, J.; Henley, R.; Bell, D. C.; Cohen-Karni, T.; Rosenstein, J. K.; Wanunu, M. Slow DNA Transport through Nanopores in Hafnium Oxide Membranes. *ACS Nano* **2013**, *7*, 10121–10128.

(33) Kundu, J.; Neumann, O.; Janesko, B. .; Zhang, D.; Lal, S.; Barhoumi, A.; Scuseria, G. E.; Halas, N. J. Adenine− and Adenosine Monophosphate (AMP)− Gold Binding Interactions Studied by Surface-Enhanced Raman and Infrared Spectroscopies. *J. Phys. Chem. C* **2009**, *113*, 14390–14397.

(34) Demers, L. M.; Ostblom, M.; Zhang, H.; Jang, N.-H.; Liedberg, B.; Mirkin, C. a. Thermal Desorption Behavior and Binding Properties of DNA Bases and Nucleosides on Gold. *J. Am. Chem. Soc.* **2002**, *124*, 11248–11249.

(35) Kimura-Suda, H.; Petrovykh, D. Y.; Tarlov, M. J.; Whitman, L. J. Base-Dependent Competitive Adsorption of Single-Stranded DNA on Gold. *J. Am. Chem. Soc.* **2003**, *125*, 9014–9015.

(36) Kowalczyk, S. W.; Wells, D. B.; Aksimentiev, A.; Dekker, C. Slowing down DNA Translocation through a Nanopore in Lithium Chloride. *Nano Lett.* **2012**, *12*, 1038–1044.

Supporting Information

S5.1 Fabrication Conditions

Table S5.1: List of metallic nanopores fabricated under different parameters. Total time-to-pore fabrication is calculated by summing the durations at which the membrane is subjected to high voltage bias. Fabrication using pulsing technique appears to introduce a high variance in fabrication time. All pores fabricated have an effective diameter less than 10-nm.

SiNx Thickness [nm]	Metal Thickness [nm]	Solution	pH	Method	Voltage [V]	Pulse Duration [ms]	Total Time-to-pore Fabrication[s]
10	30	1M KCl	10	DC	4	--	13750
10	30	1M KCl	10	DC	5	--	6250
10	30	1M KCl	10	DC	7	--	1250
10	30	1M KCl	10	DC	7	--	1600
10	30	1M KCl	10	DC	7	--	1021
10	30	1M LiCl	10	DC	14	--	2.5
10	30	1M KCl	10	Pulse	4	0.2	1.6
10	30	1M KCl	10	Pulse	5	0.2	2290
10	30	1M KCl	10	Pulse	6	0.1	154.2
10	30	1M KCl	10	Pulse	6	0.05	12.2
10	30	1M KCl	10	Pulse	10	0.1	4.5
10	30	1M KCl	10	Pulse	10	0.1	0.9
10	30	1M KCl	10	Pulse	10	0.1	1.1
30	30	2M KCl	10	Pulse	9	0.2	3.2
30	30	1M KCl	10	Pulse	12	0.2	0.8
30	30	1M KCl	10	Pulse	12	0.2	1.8
30	30	1M KCl	10	Pulse	18	0.2	41
30	30	1M KCl	10	Pulse	18	0.2	33

S5.2 Noise Characterization

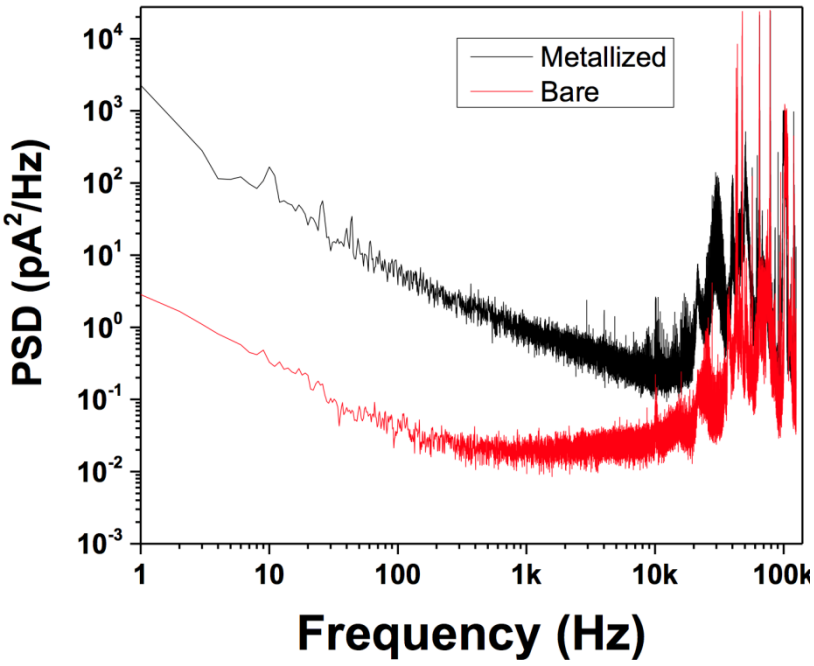

Figure S5.1: Noise Characteristic is analyzed by plotting the power spectrum density as a function of frequency. A metallized nanopore is compared with a bare SiN_x pore. Metallized pore exhibit higher level of noise in the entire frequency domain. High frequency noise can in principle be reduced by patterning the metal film to limit the area exposed to electrolyte [2,4]. The metallized pore was used in experiments to acquire data for Figure 3-5, while the bare SiN_x pore was used to acquire data for Figure 5.

S3. Software Error Rate

Table S5.2: Error introduced by software is estimated manually by sampling a subset of events for error in the evaluation of translocation time. Data points are divided into groups, base on their translocation time, and each group is examined separately. 50 separate events from each group are drawn randomly for sampling. Majority of the errors are introduced by high noise level in the current trace, preventing the software from properly detecting the beginning or the end of an event.

Translocation Time [s]	$<10^{-4}$	$[10^{-4},10^{-3})$	$[10^{-3},10^{-2})$	$\geq 10^{-2}$
# of Event Counted	1272	1084	328	103
Manually Sampled	50	50	50	50
# of mis-timed events	7	4	5	4
% Error	14%	8%	10%	8%

S5.4 Current Trace

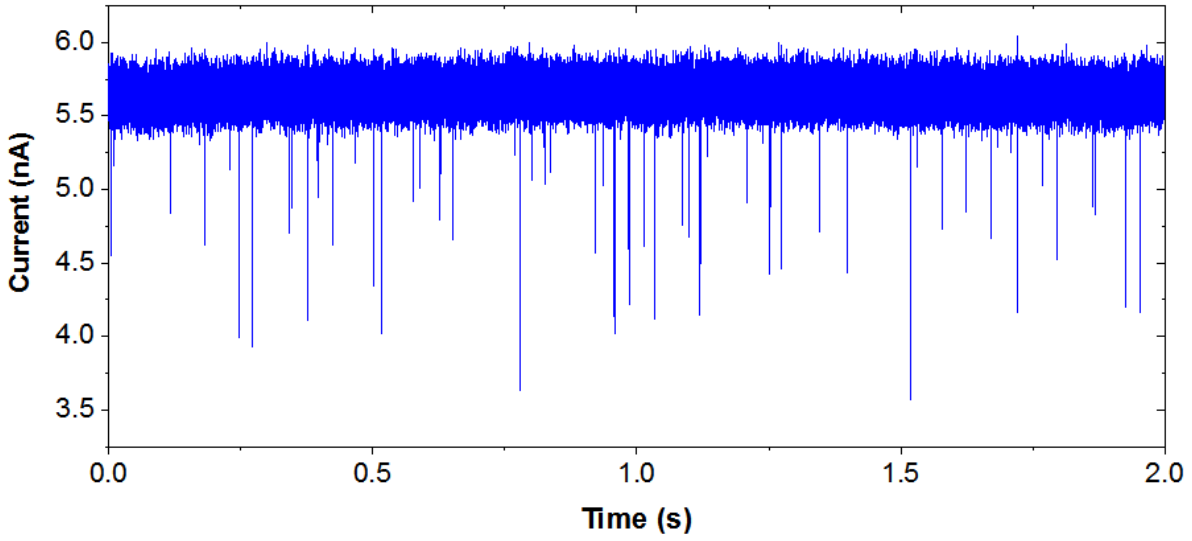

Figure S5.2: Ionic current trace showing multiple DNA translocation events through a metallized pore (d = 4.9-nm, l = 10-nm) corresponding to data shown in Figure 6a and 6c. Experiments performed with 50-nt ssDNA fragments in 3.6 M LiCl pH8, at +200 mV using an Axopatch 200B. Data sampled at 250 kHz and low-pass filtered at 100 kHz.

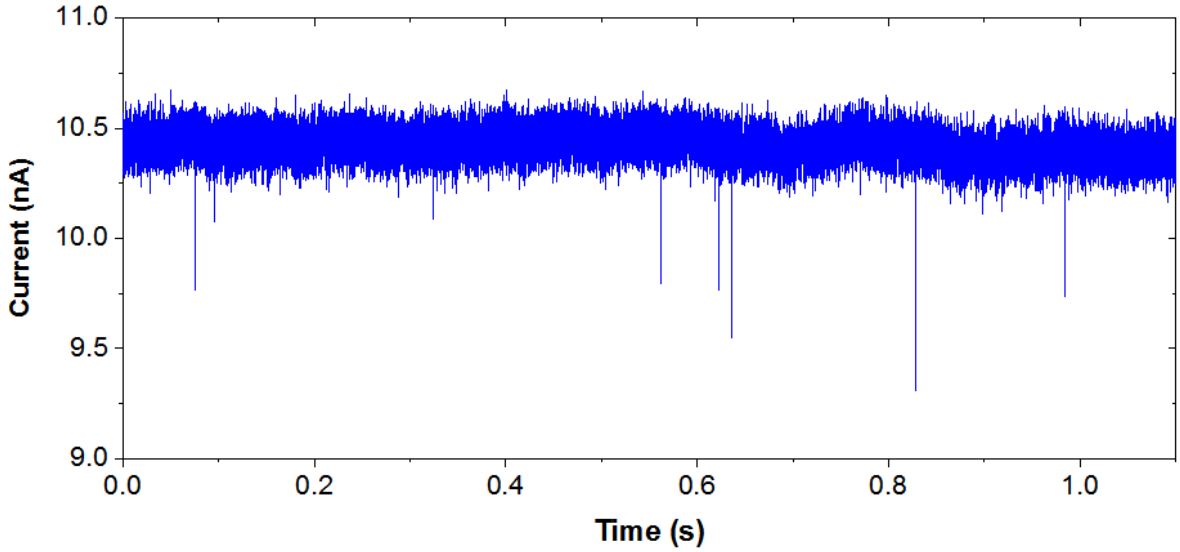

Figure S5.3: Ionic current trace showing few DNA translocation events through a metallized pore (d = 5.8-nm, l = 10-nm) corresponding to data shown in Figure 6b and 6d. Experiments performed with 50-bp dsDNA fragments in 3.6 M LiCl pH8, at -200 mV using a MultiClamp 700B with low-pass filter analog setting to by-passed. Data sampled at 750 kHz. For display purposes only, the current trace was multiplied by -1, and digitally filtered at 30kHz.

References

(1) Kowalczyk, S. W.; Wells, D. B.; Aksimentiev, A.; Dekker, C. Slowing down DNA Translocation through a Nanopore in Lithium Chloride. *Nano letters* **2012**, *12*, 1038–1044.

(2) Tabard-Cossa, V.; Trivedi, D.; Wiggin, M.; Jetha, N. N.; Marziali, A. Noise Analysis and Reduction in Solid-State Nanopores. *Nanotechnology* **2007**, *18*, 305505.

(3) Wei, R.; Pedone, D.; Zürner, A.; Döblinger, M.; Rant, U. Fabrication of Metallized Nanopores in Silicon Nitride Membranes for Single-Molecule Sensing. *Small* **2010**, *6*, 1406–1414.

(4) Krishnakumar, P.; Gyarfas, B.; Song, W.; Sen, S.; Zhang, P.; Krstić, P.; Lindsay, S. Slowing DNA Translocation through a Nanopore Using a Functionalized Electrode. *ACS nano* **2013**, *7*, 10319–10326.

Chapter 6

Conclusion and Outlook

A new nanopore fabrication technique relying on dielectric breakdown was discovered. We demonstrated that the new method is capable of producing individual nanopores down to sub-2nm. The method is shown to be superior to conventional fabrication method in cost, reliability, yield and convenience. Through performing common DNA translocation experiments, we further demonstrated that the resulting nanopores are equally compatible for biosensing applications compare to other nanopores.

To extend the understanding of the underlying mechanism, we explored different control parameters and found that the creation time is highly sensitive to applied voltage and acidity. This allows the process to be extremely rapid. We further explain the phenomenon with the percolation theory of dielectric breakdown and conclude the uniqueness of each creation event based on the stochastic property of such process. The understanding allows us to relate the fabrication process in relation to the membrane thickness and membrane area.

The future of solid-state nanopore technology will likely be integrated into a complex system. Such approach can extend functionality of a nanopore beyond pulse-resistive sensing regime. We examined the new fabrication method on its portability to metallized dielectric bilayer complex membrane. We found that the method of controlled dielectric breakdown can be deployed to create nanopore on such system. The resulting nanopore has a metallic channel concentric to the dieletric pore. The metallic channel has a conical shape with an incline toward the dielectric opening.

The metallized nanopore was found to be compatible for biosensing applications. The presence of metallic material at the vicinity of a nanopore opening can interact strongly with short ssDNA molecules. The dynamic interaction is shown to extensively prolong the translocation time of these molecules. It is also shown that the interaction favors unfolded molecules due to the long residue length outside a nanopore. It is possible such interaction dynamics can be exploited for configuration of selective filtering applications.

Future nanopore will likely have higher complexity than a bilayer system. As a proof of concept, we attempted to create nanopores with the new method on multilayer dielectric membrane with an embedded graphene electrode layer. Preliminary results indicated that it is possible to create such system, however, future work is needed to confirm such finding.

Nanopore is a versatile tool. It is one of the very limited ways for us to access and manipulate individual molecules. For this reason, the future of nanopore technology is prosperous. It is only limited by the creativity on its designs and applications. In this aspect, the new simplified nanopore fabrication method facilitated an important step toward the realization of unleashing the power of nanopore technologies.